Icarus 218 (2012) 178–195

Contents lists available at SciVerse ScienceDirect

Icarus

journal homepage: www.elsevier.com/locate/icarus

Formation of an Hesperian-aged sedimentary basin containing phyllosilicates in Coprates Catena, Mars

Peter M. Grindrod [a,b,*], Matthew West [a], Nicholas H. Warner [c], Sanjeev Gupta [c]

[a] Department of Earth Sciences, University College London, Gower Street, London WC1E 6BT, UK
[b] Centre for Planetary Sciences, University College London, Gower Street, London WC1E 6BT, UK
[c] Department of Earth Science & Engineering, Imperial College London, London SW7 2AZ, UK

ARTICLE INFO

Article history:
Received 29 June 2011
Revised 21 September 2011
Accepted 24 November 2011
Available online 6 December 2011

Keywords:
Mars, Surface
Geological processes
Terrestrial planets
Mineralogy
Spectroscopy

ABSTRACT

The extensive light-toned deposits in canyons and troughs in Valles Marineris provide evidence of formation through water-related processes. As such, these deposits offer a window to past conditions on Mars. We study a small outcrop of light-toned deposits in a closed trough in Coprates Catena, a chain of collapse pits to the south-east of the main Valles Marineris system. A well-exposed sequence of deposits on the base of the north wall of the trough offers a 220 m section for geochemical and morphologic analysis. Using CRISM data we identify the presence of both phyllosilicates and sulfates and/or opaline silica in the light toned deposits, which vary in relative strength with elevation. We observe a trend in the dominant mineralogical signal, with Al phyllosilicates occurring near the base of the deposits, both below and above a band of Fe/Mg phyllosilicates, before a transition to more sulfate- or opaline silica-rich material near the top of the section. This trend likely reflects a change in the chemistry of the water in which the deposits formed. Using a HiRISE Digital Elevation Model, we find that the layers in the light-toned deposits on both sides of the trough dip gently towards the center of the trough, with a dip direction that aligns with the strike of the trough, suggesting that the light-toned deposits formed after the trough. Our general morphologic and mineralogical observations fit well with significant amounts of water in the trough. The deposits are too small to be dated using crater counting techniques, however, our crater analysis suggests that the plains in which the trough formed are probably Late Hesperian in age. If the chemistry of the light-toned deposits reflects the primary depositional mineralogy, then this and other small troughs in Coprates Catena might provide evidence of limited phyllosilicate formation in this region towards the end of the Hesperian era on Mars.

1. Introduction

The canyons and troughs of Valles Marineris often contain distinctive, layered deposits of light-toned material (e.g. McCauley et al., 1972; Nedell et al., 1987; Lucchitta et al., 1992, 1994). These light-toned deposits (LTDs) are most often found towards the center of chasmata, and despite sometimes having heights almost as large as the surrounding canyon walls, LTDs usually show evidence of having undergone significant erosion (Lucchitta et al., 1992). A number of hypotheses have been put forward to explain the origin of these LTDs, including formation by volcanic (Chapman and Tanaka, 2001; Komatsu et al., 2004), aeolian (Peterson, 1981), lacustrine (McCauley, 1978; Komatsu et al., 1993; Lucchitta et al., 1994), or mass wasting (Sharp, 1973; Nedell et al., 1987) processes. LTDs have also been suggested to be the erosional remnants of older material that has been cut by chasmata formation (Malin and Edgett, 2000). The wide variety of LTD morphology revealed by increasingly high-resolution observations implies that multiple processes might be responsible for the formation of different LTDs. One of the most important debates regarding LTDs is determining their time of formation relative to the canyons in which they are hosted, and indeed the rest of the martian geological timescale. If LTDs predate the formation of the chasmata, then they could be Noachian in age, with their exhumation occurring later in the Hesperian (e.g. Malin and Edgett, 2000, 2001; Montgomery and Gillespie, 2005; Catling et al., 2006; Adams et al., 2009; Montgomery et al., 2009; Jackson et al., 2011). The consensus seems to prefer a LTD formation mechanism that occurs during or after chasma opening, probably during the Hesperian to Amazonian periods (e.g. Scott and Tanaka, 1986; Komatsu et al., 1993; Lucchitta et al., 1994; Schultz, 1998; Chapman and Tanaka, 2001; Fueten et al., 2005, 2008, 2010, 2011; Harrison and Chapman, 2008; Okubo et al., 2008; Flahaut et al., 2010; Okubo, 2010). Interest in LTDs in Valles Marineris has continued with the recent discovery

* Corresponding author at: Earth Sciences, UCL, Gower Street, London WC1E 6BT, UK.
E-mail address: p.grindrod@ucl.ac.uk (P.M. Grindrod).

0019-1035
doi:10.1016/j.icarus.2011.11.027

of abundant hydrated minerals within the LTDs, with the possible formation mechanisms suggesting the role of water at some point in the past (e.g. Gendrin et al., 2005; Bibring et al., 2006; Murchie et al., 2009a).

This paper addresses the formation and timing of a small outcrop of LTDs in a closed trough in Coprates Catena. Although the small size of these LTDs compared to some of the deposits in other larger chasmata has limited their observation, the advent of recent high resolution data allows us to study in detail the mineralogical and morphologic evolution of these deposits. The study trough also contains a distinctive fan deposit, suggesting the occurrence of water at some point (Di Achille et al., 2006; Weitz et al., 2006), and therefore we specifically address the question of whether the LTDs are evidence of a lacustrine environment (see Lucchitta (2009a,b), for recent summaries). The implications from the results of this study are then placed into a broader chronologic and geologic context, with the aim of contributing towards our understanding of the evolution of water on Mars.

2. Data and methods

We first prepared a Digital Elevation Model (DEM) from HiRISE stereo pair PSP_007917_1650 and PSP_009631_1650 using the method of Kirk et al. (2008). This method involves pre-processing the raw Experimental Data Records (EDRs) in the freely-available Integrated Software for Imagers and Spectrometers (ISIS) image processing routines (http://isis.astrogeology.usgs.gov), before using the commercial SOCET Set image analysis software (http://www.socetset.com) to produce a DEM with elevation postings every 1 m. This DEM was used to produce orthorectified versions of PSP_007917_1650 at 0.25 and 1 m/pixel, which served as base maps for detailed interpretation. Using the method of Okubo (2010), we assume 1/5 pixel correlations with 0.279 m/pixel in the more oblique image to determine a vertical precision of 0.19 m for our HiRISE stereo DEM. We also tied the absolute elevations in this DEM to MOLA. Where possible we carried out structural mapping of the DEM using the method of previous studies (e.g. Fueten et al., 2005, 2008; Okubo, 2010) and the Orion structural analysis software (http://www.pangeasci.com). We also produced two 20 m/pixel CTX DEMs using a similar method as above for a regional overview of the topography surrounding the immediate study area.

We analyzed a single Compact Reconnaissance Imaging Spectrometer for Mars (CRISM: Murchie et al., 2007) image that covered the study area (FRT00011DF2). Another CRISM image (FRT0000 7203) covers the fan deposit in the west of the trough, but noise levels prevented spectral signatures diagnostic of any mineral. The CRISM image used is centered at 15.02°S, 300.04°E and was taken on L_s 240.7. We used the commercial software package ENVI (http://www.ittvis.com) with the CRISM Analysis Toolkit plug-in (CAT: Pelkey et al., 2007), which is freely-available (http://crism.jhuapl.edu/CRISM_workshop_2009). We use the standard protocol for processing our CRISM data, which we outline here, but is described in detail in previous studies (e.g. Murchie et al., 2007, 2009b; Ehlmann et al., 2009; Roach et al., 2009; Lichtenberg et al., 2010). We concentrated our analysis on the near-infrared wavelengths, as these contain the most water-related absorption features. Briefly, we converted the CRISM data to I/F before applying a photometric conversion to correct for variations in illumination. We then applied an atmospheric correction using the volcano-scan method of McGuire et al. (2009), to minimize atmospheric CO_2 band absorptions. The CRISM image was then destriped and de-spiked using the CIRRUS routine in CAT, to remove noise and large spikes inherent in the instrument. Spectral parameters, which highlight visible and near-infrared spectral features in some mineral types, were generated in CAT (Pelkey et al., 2007) and, following flattening, used for initial mapping of different hydrated and/or hydroxylated terrains. The results of the spectral summary product analysis were verified by collecting spectra for specific regions of interest (RoI) by averaging a number of pixels from a single unit. These RoIs were chosen after inspection of the spectral parameter maps, as areas that best represented possible changes in mineralogy that corresponded with elevation. The absorption signatures were enhanced by ratioing against a spectrally-bland region (e.g. Bishop et al., 2009; Milliken et al., 2008, 2010; Mustard et al., 2008). To ensure that mineral identifications from RoI spectra were robust, we collected spectra from each unit from the nonmap-projected image by taking the average values of 3×3 pixels, and ratioing these spectra against 3×3 pixel averages of spectrally bland regions in the same detector column. This method of using the same detector column for the numerator and denominator in the spectral ratio reduces the chance of misidentification from detector noise (Murchie et al., 2007). The pixel locations of each set of spectra, and their accompanying bland region, are given in Table 1.

All images were georeferenced and imported into the commercial software suites ArcGIS V9.2 and V10 (http://www.esri.com), and combined with other datasets such as 128 pixel/degree Mars Orbiter Laser Altimeter (MOLA) (Smith et al., 2001) gridded data (MEGDR 128), individual MOLA tracks and shots (PEDR), and Context Camera (CTX) images (Malin et al., 2007) that are approximately 6 m/pixel. Structural analysis was carried out on the DEM and orthoimage using the commercial software ORION (http://www.pangaeasci.com) and previously-derived methods (Fueten et al., 2005) that have been successfully applied to a number of different areas and data sets (e.g. Fueten et al., 2008, 2010; Okubo, 2010).

3. Observations

3.1. Geologic context

Our study area contains LTDs within a closed trough of Coprates Catena, about 80 km south of the main Coprates Chasma rift system (Fig. 1 inset). The LTDs are located on the floor of a trough that is approximately 47 km long and 15 km wide. This trough has a minimum elevation of about 60 m, giving a total depth from the top of the trough walls to the floor to of about 3.4 km. This trough has been the focus of previous studies (e.g. Di Achille et al., 2006; Weitz et al., 2006) because of the distinctive terraced fan deposit, apparently fed by a contributory valley, which lies towards the center of the trough (Fig. 1). Although both of these previous studies suggest that the fan is a terminal deposit of fluvial activity along the incised valley, they disagree on the exact formation mechanism: Di Achille et al. (2006) argue for deposition on a sheetflood-dominated alluvial fan, whereas Weitz et al. (2006) invoke a deltaic depositional process. The implications of these different scenarios are important because they determine whether there was ever a significant standing body of water in the trough, and one of the aims of this study is to contribute to this debate.

At least three other putative valleys appear to terminate in the east of the trough, above the location of the LTDs (Fig. 1), although their level of incision is minimal in comparison with the large valley that leads to the fan deposit. For example, the large channel that terminates in the fan deposit has a depth of approximately 900 m, whereas the small channel that enters the study trough from the south above the LTDs is about 50–60 m deep. From crater-counting statistics, the plains surrounding the trough have been estimated as Hesperian in age (Scott and Tanaka, 1986), with the trough and the rest of Coprates Catena having formed later through either continuing extension of the Valles Marineris chasmata system (e.g. Weitz et al., 2006) or volcanic collapse due to subsurface dikes (e.g. Mège et al., 2003). Regardless of the exact

Table 1
Center coordinates of CRISM spectra (average of 3 × 3 pixels) in the non-map-projected cube FRT00011DF2. Pixel averaged spectra were ratioed with the bland spectra to produce the plots in Fig. 7.

Unit identifier	Average spectra pixel location		Bland spectra pixel location		Elevation (m)
	X	*Y*	*X*	*Y*	
6	435	312	435	50	489.6
5	445	311	445	50	461.7
4	457	317	457	50	445.6
3	480	327	480	50	430.7
2	497	339	497	50	423.5
1	500	331	500	50	413.3
0	496	317	496	50	404.9
DM	484	216	484	50	414.5

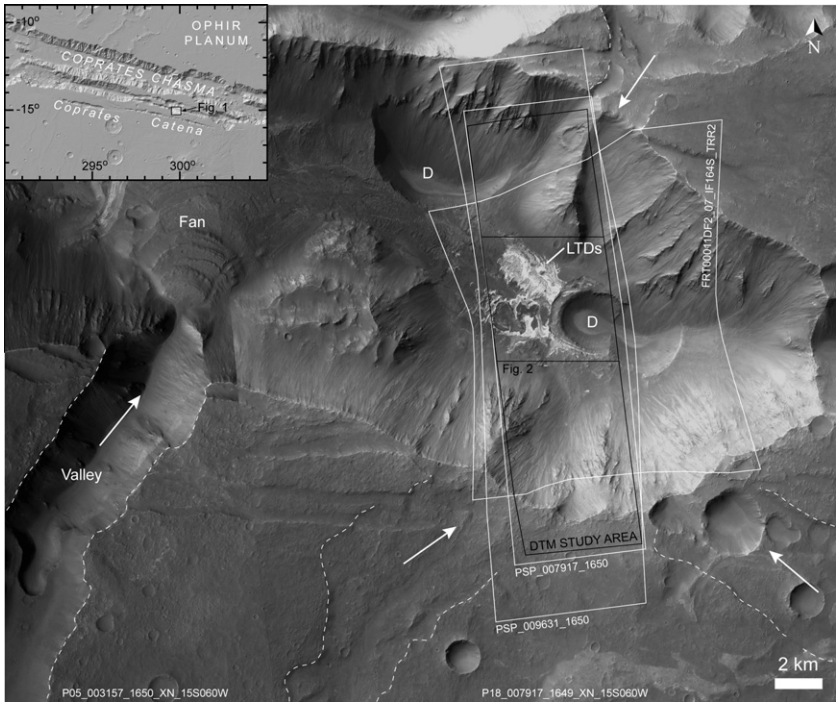

Fig. 1. Context map of the study area. Coprates Catena lies to the south of the main Coprates Chasma system (inset), and the study area is a relatively small and isolated trough at approximately 15°S, 300°W. The main image shows a CTX mosaic of the wider study region, with the valley and terraced fan studied by Di Achille et al. (2006) and Weitz et al. (2006). Collapse depressions (D) are amongst some of the youngest features in the study area. The light-toned deposits (LTDs) lie at the base of the trough, with the approximate location and direction of possible contributing plateau valley-channels shown by dashed lines and arrows respectively. Footprints of the images used in this study, as well as their image number, are given in this CTX base map. Inset is a hillshade of MOLA MEGDR (128) data.

formation mechanism of the trough it appears that significant deposition occurred after or at least contemporaneously with the formation of the trough (Di Achille et al., 2006; Weitz et al., 2006). Deposition has been followed at some stage by continuing collapse, as evidenced by the two small pits that occur within the study trough (Fig. 2), which lack impact-related features and are most likely related to collapse (Weitz et al., 2006). One of these pits cuts across the study LTDs and is an important feature in understanding the depositional mechanism and extent as it provides traceable exposures of the deposits.

The LTDs are identified as having a generally high albedo compared to surrounding material, with layers of different brightness occurring at different levels in the deposits. The LTDs are partly obscured by a dark mantling layer, and therefore the spatial extent of the LTDs might represent partial exhumation of the deposits from beneath the dark mantle (Weitz et al., 2006). Below we describe in more detail the nature of the LTDs, both in terms of their chemical and geomorphologic appearance based on CRISM and HiRISE observations respectively. We concentrate our analysis on the stratigraphy of the well-exposed LTDs on the north slope of the trough (Fig. 2) and where possible make comparisons with the deposits on the south slope of the trough.

3.2. Crism observations

We first analyze the CRISM spectral parameter summary images (Figs. 3 and 4) in order to determine the context of units identifiable in near-infrared wavelengths, before inspecting individual spectra. Fig. 3 shows the entire extent of the CRISM image area and the context of Fig. 4, which specifically highlights the LTDs. The LTDs are bright at 1330 μm, are distinct from the surrounding dusty surface (Fig. 3a), and appear to show layered variation in color in the near-infrared (Fig. 3b). Fig. 3c shows a spectral parameter summary image that highlights the depth of absorptions at 2.3 (red[1]), 2.21 (green), and 1.9 (blue) μm, which roughly correspond to near-infrared

[1] For interpretation of color in Figs. 2–10, 12 and 13, the reader is referred to the web version of this article.

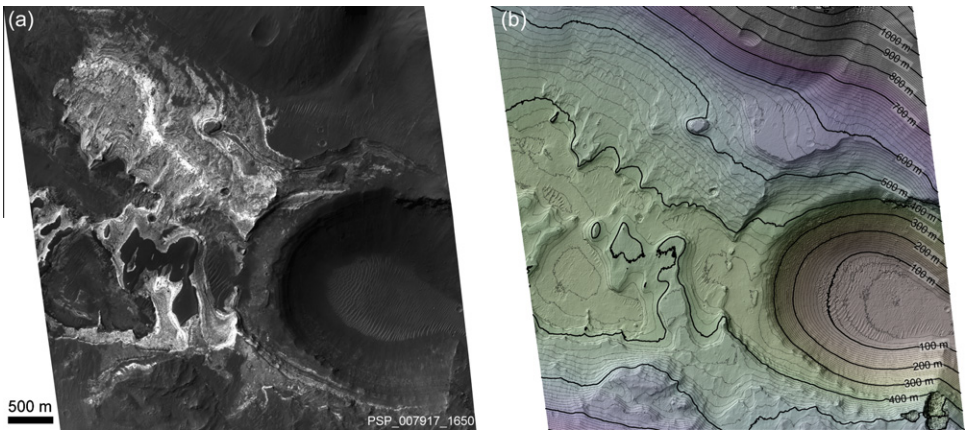

Fig. 2. Close-up of the LTD study area. (a) Orthorectified HiRISE image. (b) Colorized hillshade of the 1 m DEM made as part of this study. Contours are labeled every 100 m and drawn every 10 m. The DEM has not been edited, so that errors are clearly visible and could be avoided in any analysis. The only DEM error in this image is visible at the bottom right, leaving the study area free of errors.

signals from Fe/Mg–OH minerals, Al/Si–OH minerals, and H_2O respectively (Pelkey et al., 2007). Fig. 3d shows a spectral parameter summary image that highlights the convexity of spectra centered at 2.2–2.3 μm (red), as well as the band depth at 1.435 (green) and 1.9 (blue) μm. We set conservative stretch threshold levels for both spectral parameter summary images to highlight any possible compositional relationships at the LTDs. Fig. 3 shows that the strongest water-related signals are found in the vicinity of the LTDs, and particularly in areas devoid of the dark mantling material. We concentrate our analysis on the well-defined layered sequence in the north of the trough, and where possible compare the results with the deposits in the south of the trough.

The spectral parameter summary images (Fig. 4c and d) show that there is an apparent variation in absorption wavelength that depends on elevation, which we investigate by taking spectral profiles through the most well-defined outcrop sequence of the LTDs in the western side of the northern base of the trough (Fig. 3a). Our spectral profiles show that absorptions at 2.3 μm are concentrated in a discrete elevation band between ~400 and 440 m, whereas absorptions at 1.9 μm are concentrated from the base of our profile (~370 m) to ~480 m (Fig. 5b). Material with absorptions at 2.21 μm occur throughout the sequence, but with possible concentrations at ~390, 450, 490, and 540 m (Fig. 5b). The spectral profiles also show that the SINDEX spectral parameter is strongest at elevations from the base of our profile (~370 m) to ~580 m with a reduced occurrence at approximately 420 m and peaks at ~390 and between 435 and 500 m (Fig. 5c). In general, our spectral summary images and profiles suggest that there is a strong hydrated mineral signal at elevations from about 370 to 550–600 m, with an absence of signal between about 400 and 430–450 m, and that the strongest phyllosilicate signals occur at elevations between about 400 and 420 m.

We also took spectra at different elevations that marked out apparent spectrally-distinct units, both as 3×3 pixel averages (Fig. 6a and Table 1) and larger RoIs (Fig. 6b). In choosing the RoIs we were careful to avoid crossing any possible unit boundaries to ensure our spectra were indicative of single units (e.g. Milliken et al., 2008, 2010). We ratioed these spectra against spectrally-bland regions to highlight any absorption features in these units (Fig. 7a) for comparison with laboratory spectra (Fig. 7b). All region of interest spectra are similar to individual spectra, albeit with reduced noise, suggesting that spectral features in the RoI spectra are accurate of the true spectra, rather than the result of the averaging process (e.g. Milliken et al., 2008, 2010). All spectral ratios in the LTD sequence show absorptions around 1.9 μm, indicative of the presence of H_2O molecules, either trapped, absorbed, adsorbed, or bound in this layered sequence (e.g. Wiseman et al., 2010) and so we use other characteristic absorption features where possible to elucidate the nature of the water-containing deposits.

The general absorption trends match well with those observed in the spectral parameter summary images. At the lowest measured elevation (location 0 at 405 m), the ratioed spectrum has a primary absorption feature at 2.20 μm, with a secondary absorption feature at 1.41. Locations 1 and 2 have elevations of 414 and 424 m respectively, and are the only levels that show distinctive absorption features at 2.30 μm, with reduced absorptions at 2.2 μm. Location 3 (431 m) shows a possibly shallow absorption at 2.30 μm, with an increased absorption at 1.41 and 2.20 μm relative to locations 1 and 2. Locations 4 and 5 (446 and 462 m respectively) have distinctive primary absorption features at 2.20 and 2.27 μm, and secondary absorption features at 1.41. Location 6 (490 m) shows a broad absorption feature centered around 2.20 μm, with a secondary feature at 1.41 μm. There is also a general increase in wavelength with increasing elevation in the large absorption feature around 1.9 μm, as it shifts from 1.92 to 1.94 μm with increasing height through the sequence.

These spectral ratio trends, together with the spectral parameter summary images, point to a changing chemistry recorded in the LTDs. The primary characteristics that we use to monitor this change are the relative strength of absorptions at wavelengths around 2.20 and 2.30 μm; absorptions around 2.20 μm can be caused by OH bond vibrations in Al-rich phyllosilicates, whereas absorptions around 2.30 μm can be the result of OH bound to Fe and/or Mg (e.g. Hunt and Ashley, 1979; King and Clark, 1989; Bishop et al., 2008; Warner and Farmer, 2010; Wiseman et al., 2010). Opaline silica also has a distinctive Si–OH absorption band between 2.21 and 2.26 mm (Milliken et al., 2008), which tends to be a broad absorption centered at longer wavelengths than Al–OH bond vibrations in Al-rich phyllosilicates (Mustard et al., 2008). From the base of the LTDs (~350 m) to about 410 m (Spectrum 0) the CRISM data suggest the presence of general hydrous minerals, with the absorption feature at 2.20 μm possibly indicative of Al phyllosilicate group minerals such as montmorillonite or kaolinite. A subtle absorption feature at 2.35 μm also found at these lowest elevations in the sequence might be indicative of illite. At elevations between about 410 and 425 m (Spectra 1 and 2), the marked increase and decrease in absorption at 2.30 and 2.20 μm respectively suggests that Fe- and/or Mg-rich phyllosilicates, such as nontronite or saponite, could be dominant. At elevations between about 425 and 445 m (Spectrum 3), the 2.30 μm absorption has become less

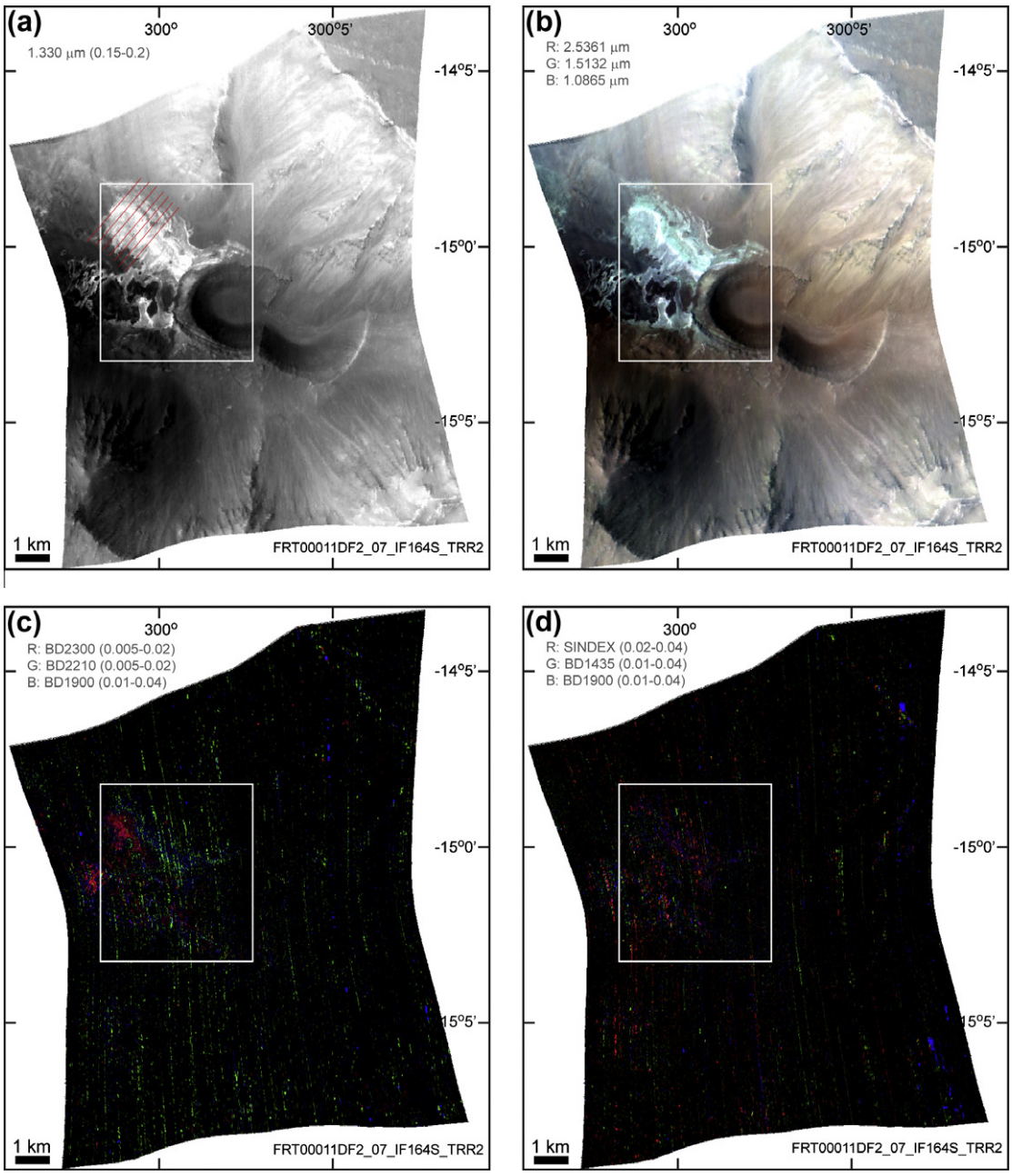

Fig. 3. The CRISM cube (FRT00011DF2) used in this study. (a) Grayscale image (1330 μm) showing the location of the LTDs, canyon walls and collapse depressions (D). Also shown are the locations of the spectral profiles averaged in Fig. 5 (red lines). (b) Near-infrared image with the color planes R = 2.54 μm, G = 1.51 μm, and B = 1.09 μm. (c) Spectral parameter summary image showing phyllosilicate trends, with the color planes R = D2300, G = BD2210, and B = BD1900. (d) Spectral parameter summary image showing hydrated mineral trends, with the color planes R = SINDEX, G = BD1435, and B = BD1900. In each image north is to the top, and where appropriate the threshold stretch is given in brackets for each color plane. The white box shows the location of Fig. 4.

significant than the well-defined 2.20 μm absorption, suggesting a transition to Al-rich phyllosilicates, although the general spectral shape between 1 and 2 μm could suggest the continuing presence of nontronite. At elevations between 445 and 480 m (Spectra 4 and 5) are similar to the "hydrated silicates" of Roach et al. (2010), attributed to acid-leached phyllosilicates or a smectite–jarosite mixture. At elevations above about 480–500 m (Spectrum 6), the broad absorption at 2.21 μm, possible absorption at 2.41 μm and the gradual transition of the absorption center from 1.92 to 1.94 μm could be indicative of a sulfate hydrate-dominant layer, such as gypsum or epsomite. However, the relative weakness of the 2.21 μm to the 1.9 μm absorption in gypsum could imply that Si–OH absorptions are responsible for the spectral features at these elevations, possibly suggestive of opaline silica. Regardless of the precise mineralogical changes, there appears to be a general trend in our LTDs of phyllosilicates occurring at the lowest elevations, with a change to sulfate- or silica-dominated mineralogies at the higher elevations.

We also use the spectral parameter summary images to investigate the nature of the LTDs away from the well-defined northern wall deposits. However, as deposits elsewhere are less well-defined and sometimes extend beyond our stereo-derived DEM, our analyses in these regions are inherently less conclusive. The strongest phyllosilicate signals occur in the central west region of the trough, with only a small area covered by HiRISE stereo coverage and hence our DEM. This region appears red in the phyllosilicate parameter image (Fig. 3c), similar to the area in the north of the trough, and thus contains material that has a strong absorption at 2.30 μm.

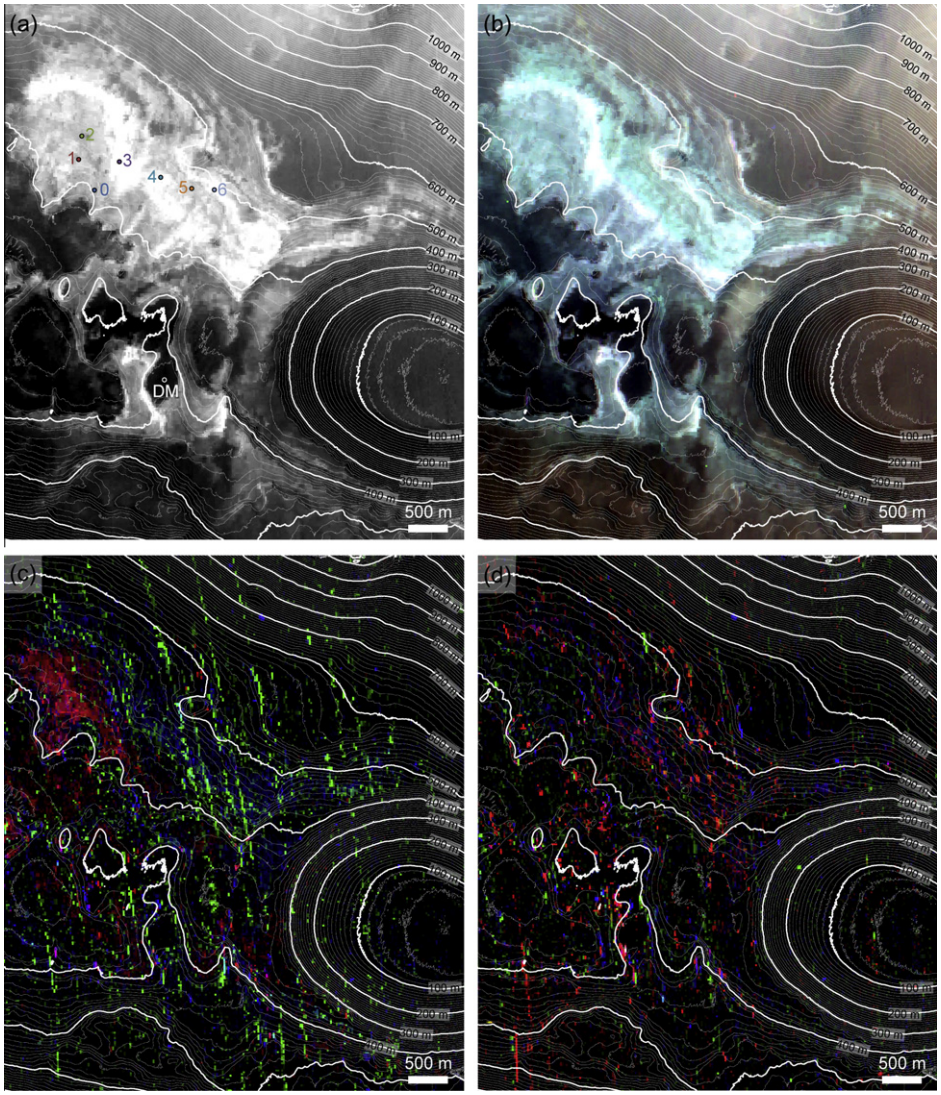

Fig. 4. Detailed CRISM images combined with the DEM of the study area. (a) Grayscale image (1330 μm) with elevation contours overlain. Also shown are the locations of the spectra shown in Figs. 6 and 7. (b) Near-infrared image with the color planes R = 2.54 μm, G = 1.51 μm, and B = 1.09 μm. (c) Spectral parameter summary image showing phyllosilicate trends, with the color planes R = D2300, G = BD2210, and B = BD1900. (d) Spectral parameter summary image showing hydrated mineral trends, with the color planes R = SINDEX, G = BD1435, and B = BD1900. In each case contours are labeled every 100 m and drawn every 10 m.

Analysis of a CRISM spectra for a RoI of 27 pixels yields profiles that are similar to locations 1 and 2, with a primary absorption at 2.3 μm, suggesting the dominant presence of Fe and/or Mg phyllosilicates. The part of this area that is covered by the DEM gives an elevation range that is lower than the similar area in the north of the trough, with a range of occurrence of between 380 and 390 m. Most of the remainder of the LTDs in the central and southern part of the trough are lacking phyllosilicate signals in the spectral parameter images, and instead show similarities with location 6 on the northern part of the trough. In general there appear to be some similarities between deposits in the well-defined northern exposure of the LTDs and the LTDs found elsewhere in the trough, suggesting possibly similar formation mechanisms.

3.3. HiRISE observations

We used the HiRISE DEM and orthoimage to study the morphology and stratal geometry of the layered stratigraphy. We first carried out structural analysis of layered deposits where possible, using a plane-fitting method that returns the dip and strike of the surface (e.g. Fueten et al., 2005, 2008; Okubo, 2010). We limited our analysis to those layers that had mean dip errors smaller than the dip angle (Okubo et al., 2008), and thus determined the dip and strike of 60 separate layers in 12 different locations (Fig. 8a). The correlation coefficient and goodness of fit for all orientations are 0.97% and 93.5% respectively, which were measured over length scales ranging from 54 to 731 m, with a mean trace length of 266 m. The general direction of strike of the bedding mimics that of the orientation of the trough with a mean strike of 106° (Fig. 8b). Measurements of the bedding orientation reveal that layers on both sides of the trough generally dip gently to the center of the trough, with dip angles of between 1° and 13°, mimicking the slope trend of the trough walls (Fig. 8c). These low dip angles mean that the true thickness of the layers is similar to the apparent thickness. Our orientation measurements suggest that strata at higher elevations along the northern trough margin generally have larger dip angles (Fig. 8d); it is difficult to establish this relationship on the southern wall of the trough.

Secondly, we used the 25 cm/pixel orthorectified HiRISE image PSP_007917_1650 to identify morphological features that allowed us to define units that correlate with the CRISM spectra locations. In ascending elevation order, and corresponding to their equivalent

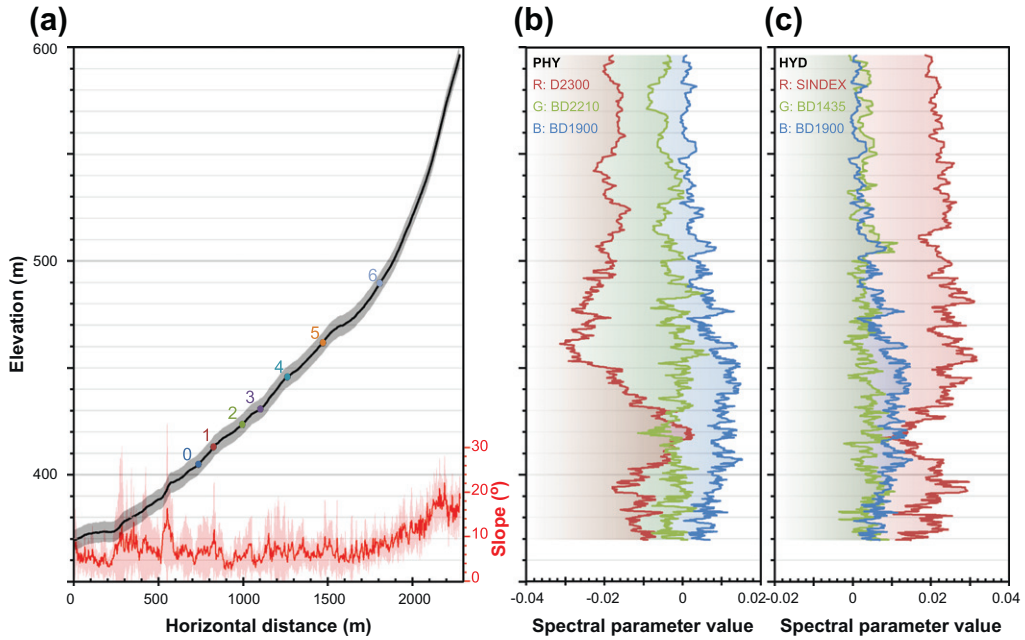

Fig. 5. Spectral parameters as a function of elevation. The seven profiles shown in Fig. 3 were used to take mean values of elevation, slope, and spectral parameters in Fig. 3c and d. (a) Topographic profile of the northern section of the LTDs. The solid black line is the mean and the gray region is the standard deviation of the seven profiles. Vertical exaggeration is 11 times. The elevations of the spectra shown in Figs. 6 and 7 are also shown. The corresponding slope values are also shown in red, with both the mean (solid red line) and standard deviation (red region) given. (b) The phyllosilicate-related spectral parameters as a function of elevation, corresponding with the profile given in (a). The colors correspond to the bands in Figs. 3c and 4c, and are shown at the top left. (c) The hydrated mineral-related spectral parameters as a function of elevation, corresponding with the profile given in (a). The colors correspond to the bands in Figs. 3d and 4d, and are shown at the top left. In both (b) and (c) the values represent the mean values of the seven profiles. The standard deviation plots are not shown for clarity, but follow a similar trend to the mean.

CRISM spectrum identifying number, these units are: Pavement Lower (Pa_L); (CRISM 0) Layered Lower (La_L); (CRISM 1) Pavement Intermediate (Pa_I); (CRISM 2) Pavement Upper (Pa_U); (CRISM 3) Pavement Bright (Pa_B); (CRISM 4 and 5) Layered Channeled (La_C); and (CRISM 6) Layered Upper (La_U). These units are defined primarily on their appearance on the north wall of the trough but, where possible, were traced as far as possible to the south wall. We have created a schematic graphic section (Fig. 9) to summarize the main features of the units, which are described in more detail below. Overall we see no evidence for specific geomorphologic features that correspond to specific spectral features, but rather layering and fracturing that are common to all spectral units.

The lowest unit that can be identified in the LTDs, with an elevation of 356 ± 12 m is Pa_L. Exposures of this unit are revealed by the large (>2 km in diameter) collapse pit in the east of the trough (Fig. 8a). Pa_L is frequently obscured by both a dark mantling material (DM), which appears as a thin coating of dark (spectrally bland) material, and also by isolated dune-forming dark material. These obscuring materials hinder identification of sub units with Pa_L, but the majority of this unit appears as an intermediate-toned material fractured on a scale of 1–2 m (Fig. 10a). This distinctive fractured surface is partially visible through the DM material, suggesting that, at least in some locations, this mantling material is thin. Where clearly visible, Pa_L shows little variation in fracture pattern and little to no evidence of layering except to the northwest of the trough study area, where a limited exposure of layered material is visible. This exposure is about 15 m thick, with sub-meter bedding layers arranged in at least four bundles ~3–4 m thick (Fig. 10a) that appear to have a similar dip and dip direction to the rest of the LTDs (Fig. 10b) but might form a sub unit to Pa_L.

The Layered Lower (La_L) unit has mean lower and upper contact elevations of 389 ± 6 and 410 ± 4 m respectively, giving a mean thickness of about 20 m. This unit generally consists of light-toned layered material with sub-rectangular fracturing creating blocks less than 1 m to over 5 m in diameter (Fig. 10a). This unit shows the most sub-units, with nine possible individual layers, ranging from about 1 to 5 m in thickness, and with some variation between layers in terms of brightness, fracture density and overall texture. Layers measured in this unit are close to horizontal, with a mean dip of 2.2 ± 1.4° and a mean dip direction of 100 ± 40°. The lower contact might be a gradual transition to fractured material in Pa_L, although it appears well-defined in places due to the edge of a thin mantling material.

The contact between La_L and Pavement Intermediate (Pa_I) is a gradual transition to similarly fractured material that is generally darker and lacking in layers. The mean lower and upper contact elevations are 410 ± 4 and 404 ± 13 m respectively, due to this unit only outcropping in the west of the northern wall and therefore having an upper contact that is limited, thus producing a mean upper value that is less than the lower value. However, in a single profile through this unit (Fig. 9) the thickness is approximately 22 m. Pa_I consists of a single unit of mostly sub-rectangular fractured material that has an erosional texture consisting of scallops (~20 × 30 m) in some areas to the west of the outcrop. No layers could be used for structural analysis in this unit. Pa_I has an overall darker appearance (Fig. 10c) than the units both below and above. This well-defined transition from dark to light material marks the contact with the Pavement Upper (Pa_U) unit above and the shift in CRISM absorption features from 2.3 to 2.2 μm (Fig. 10c).

The Pavement Upper (Pa_U) unit has mean lower and upper contact elevations of 404 ± 13 and 429 ± 9 m respectively, giving a mean thickness of about 25 m across the entire unit. This unit has a similar appearance to Pa_I, albeit with an increased overall brightness (Fig. 10c). At least one possible sub-unit is present as a thin (~1 m) dark band in otherwise continuously fractured pavement material (Fig. 10c). There are several possible other sub-units in the west of this unit that have not been included in Fig. 9 as they

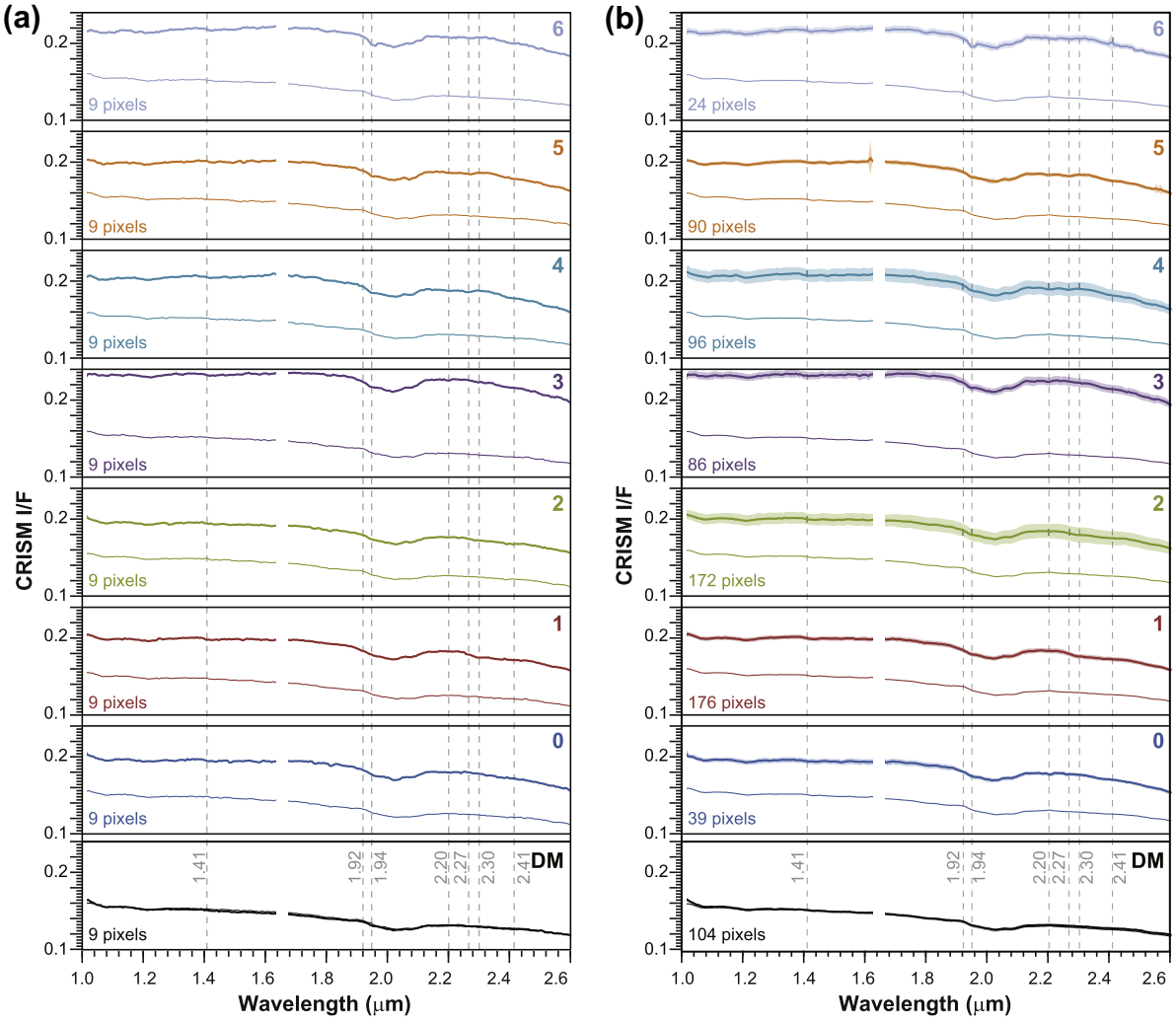

Fig. 6. Numerator and denominator spectral pairs used in CRISM ratios. (a) Individual spectra (3 × 3 pixel average) taken at the locations indicated in Fig. 4a, and (b) spectra taken over larger Regions of Interest (RoI) of the same unit (pixel average varies). In each case the thick line represents the numerator and the thin line the denominator. For the RoI spectra the standard deviation of the numerator is also given by a shaded region. Data are not shown at around 1.00 and 1.65 μm due to known instrument artifacts (e.g. Fueten et al., 2010; Lichtenberg et al., 2010). Dashed vertical lines correspond with absorption wavelengths in Fig. 7.

are limited in extent and only the thin dark layer is visible at other areas of this unit. The upper contact with the Pavement Bright (Pa_B) unit is often a gradual textural transition, although in some places to the west it is marked by scalloped structural features similar to those visible in Pa_I.

The Pavement Bright (Pa_B) unit has mean lower and upper contact elevations of 429 ± 9 and 452 ± 11 m respectively, giving a mean thickness of about 22 m across the entire unit. There are five separate layers in Pa_B, forming possible sub-units, with the lower two layers having a fracture texture similar to that of Pa_U. The largest layer in Pa_B, approximately 5 m thick, has the lowest fracture density of any material in the LTDs, and although parallel fractures with a spacing of about 5–10 m are visible, the bulk of this layer has not broken up into individual blocks (Fig. 11a), as in other unit layers. The contacts with the units both below and above Pa_B are gradational, with transitions occurring in regions of increased block density at both boundaries.

Above Pa_B is the Layered Channeled unit (La_C), which has a distinct appearance amongst all of the unit layers on the north wall of the trough. The mean lower and upper contact elevations of La_C are 452 ± 11 and 489 ± 16 m respectively, giving a mean thickness of about 37 m across the entire unit. There are possibly three separate layers in La_C, although individual layers are again only well-defined in the west of the outcrop. Most of the possible sub-unit layering contains channel-like features, approximately 10–20 m in width and less than 200 m in length, which are of the order of 1 m in depth (Fig. 11b). These channel-like features cut through all the possible sub-unit layers and are unique to La_C. Layers in La_C have a blocky texture, with individual blocks less than about 5 m in diameter, and varying brightness giving an overall appearance similar to the La_L unit, albeit with the addition of the channel-like features.

The boundary between La_C and Layered Upper (La_U) is well-defined by a sharp contact between relatively dark material that contains the channel-like features (La_C) and relatively bright material with sub-horizontal layers and an absence of channel-like features (La_U) (Fig. 11c). The mean lower and upper contact elevations of La_U are 489 ± 16 and 577 m respectively, giving a mean thickness of about 88 m across the entire unit. There five possible sub-unit layers, ranging from about 4 to 47 m in thickness, although at least one of these sub-units contains fine layering on a sub-meter scale that is well-defined in the west and east of the outcrop. These small-scale layers are defined by their varying brightness and fracture density and can be traced across almost the entire 4.5 km long outcrop. In the west of the outcrop these fine layers had a measured dip of between 3° and 5°, whereas in the east the measured dip of the layers was between 7° and 13°. The strike of the fine layers remains between about

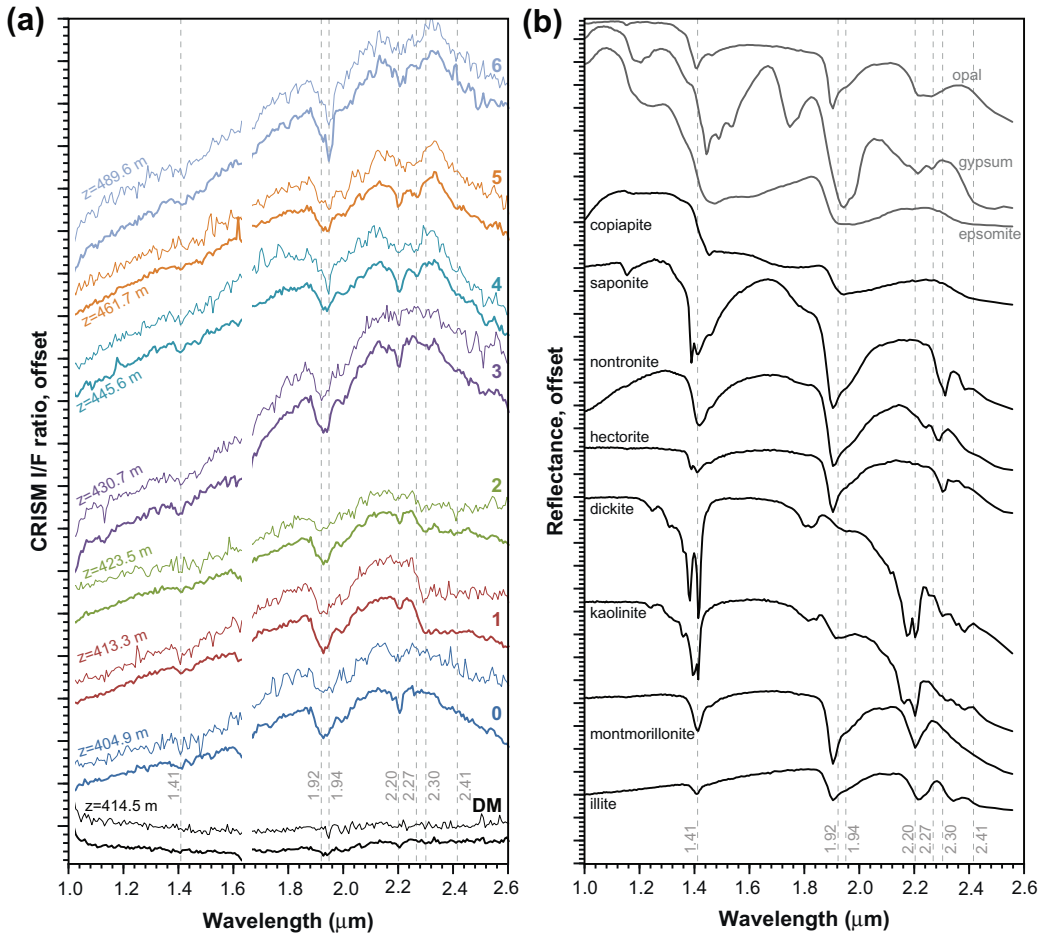

Fig. 7. CRISM spectral ratios and comparison mineral reflectance spectra. (a) CRISM ratios made using the numerator and denominators shown in Fig. 6, taken at the locations shown in Fig. 4a. Thick lines represent the RoI spectra and thin lines represent the individual spectra (3 × 3 pixel average). For each ratio the elevation at the pixel average location is also given. DM is the dark mantling material discussed in the text and does not form part of the CRISM sequence study. Data are not shown at around 1.00 and 1.65 μm due to known instrument artifacts (e.g. Fueten et al., 2010; Lichtenberg et al., 2010). Dashed vertical lines correspond with absorption wavelengths used for identification. (b) Laboratory reflectance spectra of candidate minerals showing probable species responsible for low elevation (black lines) and higher elevation (gray lines) spectral features. All spectra are from the USGS spectral library splib06a (Clark et al., 2007), with reference spectra for illite (GDS4), montmorillonite (SWy-1), kaolinite (CM9), dickite (NMNH106242), hectorite (SHCa-1), nontronite (SWa-1.a), saponite (SapCa-1), copiapite (GDS21), epsomite (GDS149), gypsum (HS333.3B), and opal (TM8896).

80° and 100° in both the west and the east of the outcrop. The contact between La_U and the overlying dark mesa (DM) material is well-defined for the majority of its length (Fig. 11c), except where dark material has either buried (west of the outcrop) or been eroded (center of the outcrop) to obscure the boundary. The removal of DM material to reveal La_U in the center of the outcrop demonstrates the relative thinness of this unit in this region. The DM material contains both impact craters and aeolian bedforms, indicating possibly two separate components make up the dark material.

Although some HiRISE units can be traced through the center of the trough and into outcrops on the south wall, the overall exposure in these regions is poor compared to the north wall and thus limits our analysis. Nonetheless we have identified some units in these regions with similar textures, overall morphology and contact elevations to those identified on the north wall. A possible contact between Pa_U and Pa_B on the south wall is observed at an elevation of 426 ± 5 m, matching well with the similar contact on the north wall. The likely observable extent of LTDs on the south wall have an elevation of approximately 570–575 m, matching well with the upper boundary of LTDs on the north wall. No LTDs are seen above this level, apart from one small (~80 × 200 m) isolated outcrop of possible light-toned material at an elevation of ~650 m.

3.4. Crater counting survey

In order to determine the age of the LTDs, we conducted a crater counting survey for units both interior and exterior of the study trough using HiRISE and CTX images (Fig. 12). We first counted all craters visible to the limit of resolution in the orthorectified HiRISE image (3–4 pixels, equivalent to ~1 m craters) to gauge an overview of the crater density of different surfaces (Fig. 12a). Notable surfaces with a high crater density include the cratered plains outside of the main study trough, but also dark mesa material above the main outcrop of LTDs. The cratered plains show an area of relatively low crater density that appears to be aligned with the eastern extent of a possible small channel that appears to flow into the trough (Fig. 1). Dark mesa material that partially obscures some LTDs also shows a marked increase in crater density compared to the low crater density LTDs.

We used the crater density map to guide selection of representative units for more quantitative crater analysis. We selected four main crater units, including the LTDs, a small outcrop of dark mesa material, the cratered plains material outside of the trough, and the low crater density channel region that cuts the cratered plains. Several factors hinder us from making confident statements about absolute age from our HiRISE crater statistics. Although we counted just over 55,000 craters in the HiRISE image, 60% were less

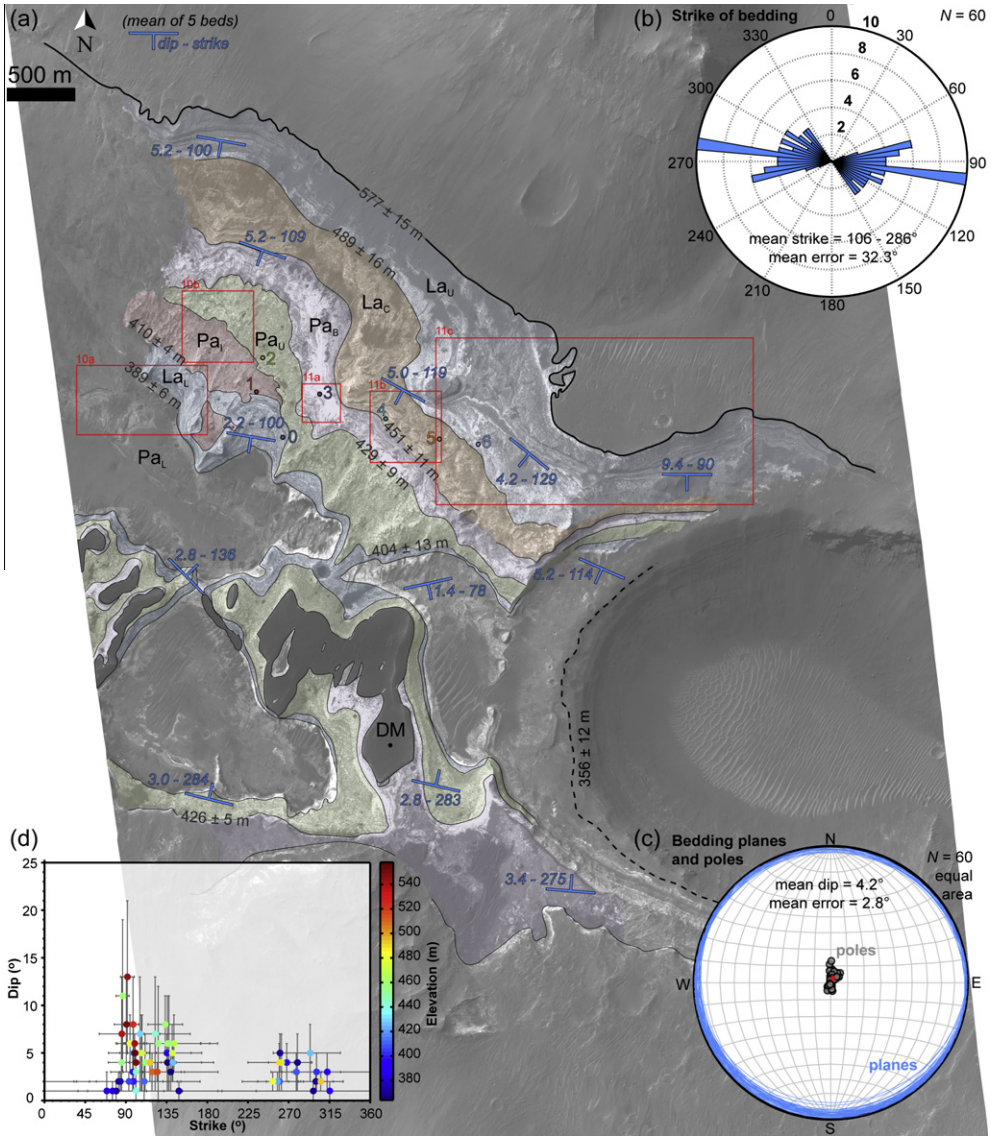

Fig. 8. Structural analysis from HiRISE observations. (a) HiRISE basemap (orthorectified image PSP_007917_1650) showing the approximate location of the upper (solid thick line) and lower (dashed thick line) boundaries of the LTDs with their accompanying mean elevation (±standard deviation). Also shown are the approximate locations of the main stratigraphic units (colored units separated by thin lines), and the positions of the CRISM spectra (colored dots and numbers). The units are Pa_L (Pavement Lower), La_L (Layered Lower), Pa_I (Pavement Intermediate), Pa_U (Pavement Upper), Pa_B (Pavement Bright), La_C (Layered Channeled), La_U (Layered Upper), and DM (dark mesa). Also shown are the dip and strike of the bedding at that location, with five strike and dip measurements taken on different beds in each case. Red boxes indicate the position of subsequent images. (b) Rose diagram showing the strike of all (60) beds measured in the structural analysis. (c) Lower-hemisphere equal-area stereographic projection of the poles to all measured beds (gray circles), with the mean pole also shown (red circle). Also shown are the planes of the beds (blue lines) that correspond to the poles, and the mean and standard deviation values of the dip of all beds. (d) Plot showing the relationship between strike, dip and elevation of all measured beds. For each point the error in the measurements of strike and dip are also given (gray error bars).

than 5 m in diameter and thus formed part of the crater population downturn inherent in studies of small craters (e.g. McEwen, 2003; Hartmann, 2005; McEwen et al., 2005). Secondly, only five craters in the HiRISE image are greater than 100 m in diameter, meaning that there are probably large uncertainties inherent in any inferred ages (Hartmann, 2005). Finally, the possible burial and erosional history of the area (see Section 4) could also introduce significant absolute age errors in this area (e.g. Malin and Edgett, 2001, 2003). Therefore we refrain from inferring absolute ages from our HiRISE crater counting survey, and instead note the possible relative age relationships (Fig. 13a) that the LTDs might have a younger crater retention surface than the dark mesa material, which might in turn be younger than the cratered plains material. It is also possible that the exhumation of units could create an inverse crater density relationship, where the youngest units that were first exposed contain the highest density of craters relative to the lowest units in the sequence.

We used CTX images to estimate absolute crater count ages, but the small area of LTDs and dark mesa material limited our study to surfaces outside of the main study trough. We counted 14,234 craters in three representative areas of the cratered plains surrounding the trough, encompassing 1402 km^2. Using the cratering model of Hartmann and Neukum (2001), and the production function of Ivanov (2001), we determine a crater retention age of the cratered plains of approximately 3.16 Ga (Fig. 13b), for craters between 355 m and 1.26 km in diameter, which matches well with the Hesperian age determined by Scott and Tanaka (1986), who counted all craters across the extent of this unit with $D > 5$ km, and Schultz (1991), who counted all craters with $D > 1$ km. Therefore the cratered plains outside of the study trough appear to be

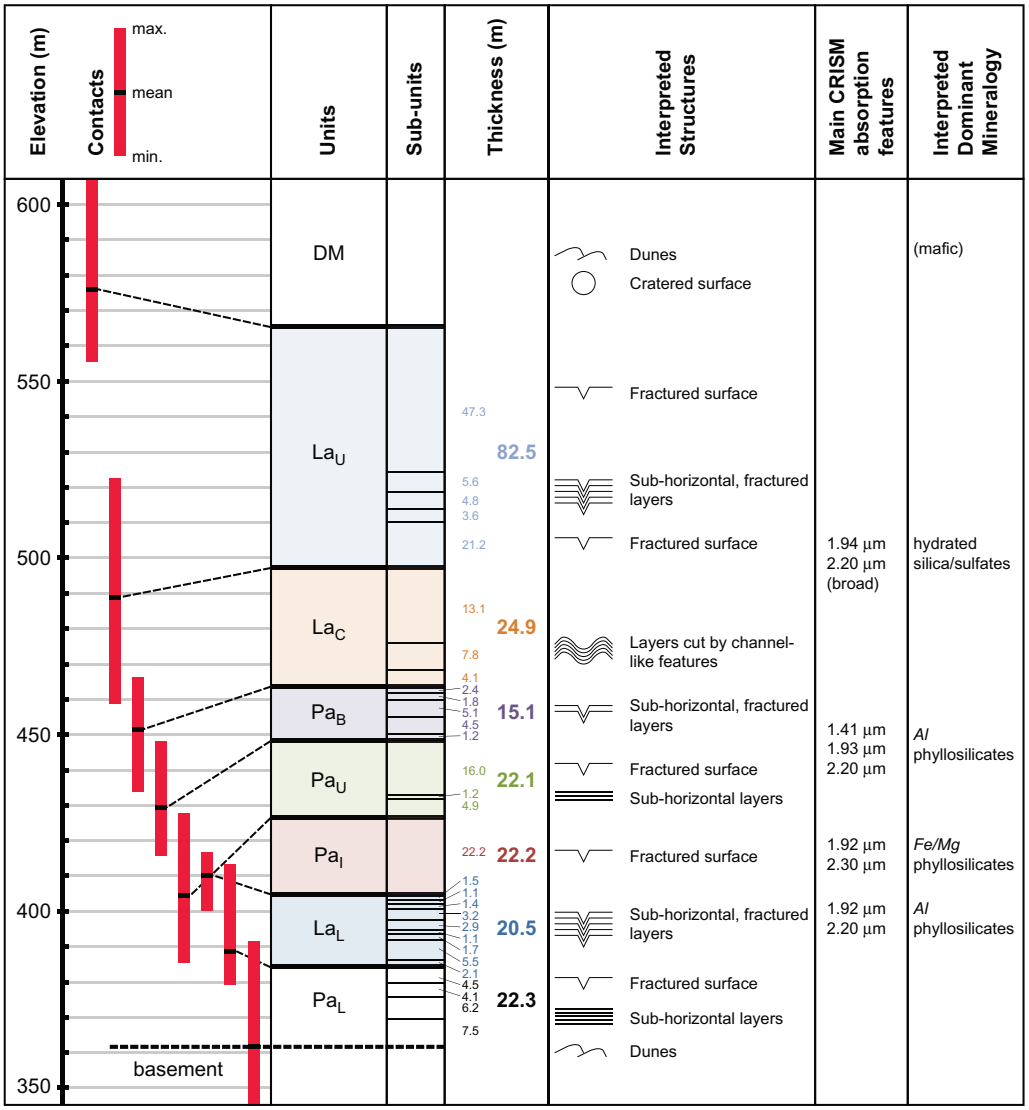

Fig. 9. Graphic sedimentary log of LTDs in the northern wall of the Coprates Catena trough. Elevation contacts (mean, minimum, and maximum) are calculated for the entire contact on the northern wall, whereas the elevation values for the units are taken from a single profile shown in Fig. 5a. Thicknesses of units and possible sub-units are measured from the single profile, whereas the structures and main CRISM absorption features are representative of the unit as a whole.

Late Hesperian in age, even when possible crater count errors are considered. We counted 294 craters in two areas representative of the channel cutting through the cratered plains unit and entering the trough, covering an area of 71 km^2. In this unit, for craters with diameters between 335 and 455 m, we determine a crater retention age of 3.1 Ga, which matches well with the inferred age of the cratered plains. A sharp kink in the fit suggests a crater resurfacing event, and so for craters between 150 and 195 m in diameter we determine a crater retention age of approximately 605 Ma. However, this implied Late Amazonian-aged resurfacing event is based on a fit to only nine craters due to the limited areal extent of this unit, and therefore we do not place confidence in this absolute age, but instead note a crater resurfacing event sometime after formation of the cratered plains. Although these units are much larger in area and do not directly affect our study LTDs, they allow us to place into a larger chronologic context the local processes described above and discussed below.

4. Discussion

In this section we combine the CRISM and HiRISE observations in order to discuss the overall history of the LTDs, focusing in particular on (1) the relative and absolute timing of trough formation and deposition of the LTDs, (2) possible formation mechanisms for the observed layered units and hydrated minerals, and (3) the possible wider implications for aqueous processes on Mars.

4.1. Timing of LTD and trough formation

The overall geomorphology and mineralogy of the LTDs in Coprates Catena suggest that they are relatively thin deposits that are draped on the lower walls and floor of the trough. The structural analysis indicates that the layers exposed at the center of the trough have shallow dips. Furthermore, the measurements suggest a systematic increase in dip (up to 15°), moving towards the margins of the trough. The strike of the LTDs also matches well with the orientation of the long axis of the trough, suggesting that the LTDs were deposited after the main opening and mimic the structure of the pre-existing and underlying walls and floor of the trough. The overall pattern of possibly identical deposits, identified in both HiRISE and CRISM observations, occurring at similar elevations on both sides of the trough suggests that the corresponding layers might be similar depositional units.

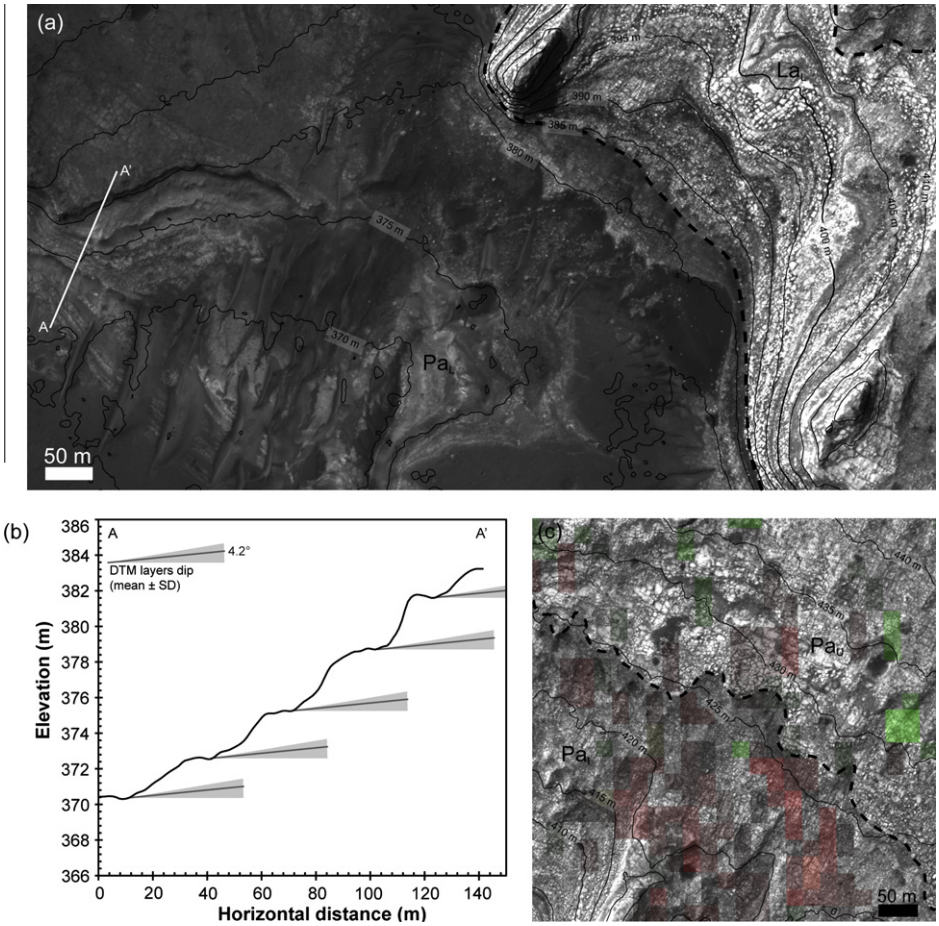

Fig. 10. HiRISE observations of LTDs in the lower part of the north wall of the trough. (a) LTDs units Pavement Lower (Pa_L) and Layered Lower (La_L). (b) Topographic profile through layered material towards the base of Pa_L, showing a consistent dip angle. For comparison, gray lines show the mean dip of all layers in the study area, with the standard deviation shown by the shaded gray areas. (c) LTDs units Pavement Intermediate (Pa_I) and Pavement Upper (Pa_U), with CRISM phyllosilicate parameters overlaid (Red = D2300, Green = BD2210). Both images are taken from PSP_007917_1650 with north to the top of the images and 5 m contour intervals. In each image the dashed lines represent approximate boundaries between the units.

The absence of evidence for faulting and folding in the LTDs and the draping characteristics of the layers within the trough indicate that the main collapse of the trough occurred before LTD deposition, and argue against the LTDs being an extensive bedrock layer that has been cut through and exposed by trough formation (e.g. Malin and Edgett, 2000; Catling et al., 2006), or syn-collapse deposits (e.g. Fueten et al., 2008). However, some limited collapse has occurred after LTD formation, as demonstrated by the presence of collapse pits at the base of the trough, suggesting the LTDs could have formed after the main trough opening but before the final stages of limited collapse. Given the age constraints for trough formation in this region presented in this analysis and previous studies (Scott and Tanaka, 1986; Schultz, 1991), we suggest that the LTDs were likely deposited at some point after the Late Hesperian to Early Amazonian. The small area of the LTDs themselves, and their likely burial and exhumation, means that crater counting-derived ages are unreliable (Fig. 13a). Crater counting of the LTDs is further hampered by the possibility that at least some of the putative craters in these hydrated materials might be the result of karstic dissolution, rather than impact, processes (e.g. Baioni and Wezel, 2010; Grindrod and Balme, 2010). However, our crater model ages derived for the cratered plains outside of the trough, which do not show evidence of significant erosion since formation, indicate a Late Hesperian age (3.2 Ga). Exactly how long after the plains Coprates Catena formed is difficult to determine, but if it is related to the wider Coprates system as part of the opening of Valles Marineris, then the majority of collapse might have occurred as late as the Early Amazonian (Schultz, 1998). We note that there probably was at least one crater resurfacing event in the small channel areas of the cratered plains, but do not assign an absolute age for this event(s). The comparable crater densities in the cratered plains and dark mesa material, and the unit that we interpret to be the pre-LTD trough base, suggests that either (1) LTD formation was relatively short in duration compared to the age of the other surfaces, or (2) that the LTD crater retention age has been significantly affected by erosion, presumably as a result of their inherent weakness, particularly if they have high porosities (e.g. Grindrod et al., 2010).

4.2. Origin of the LTDs and hydrous phases

A key question for the origin of LTDs is whether the observed hydrous mineral phases within Coprates Catena represent in situ hydrous alteration or externally-derived detrital materials (Bristow and Milliken, 2011). In the former hypothesis, the hydrous mineral-bearing units formed within the trough, in the presence of water. The observed vertical transition in mineralogy may therefore represent a change in water chemistry, whereby the lower phyllosilicate-bearing units indicate a neutral pH aqueous alteration environment and the higher sulfates or opaline silica suggest a later-stage transition to acidic conditions. With the in situ alteration hypothesis, the relative chronology of the hydrous phases can

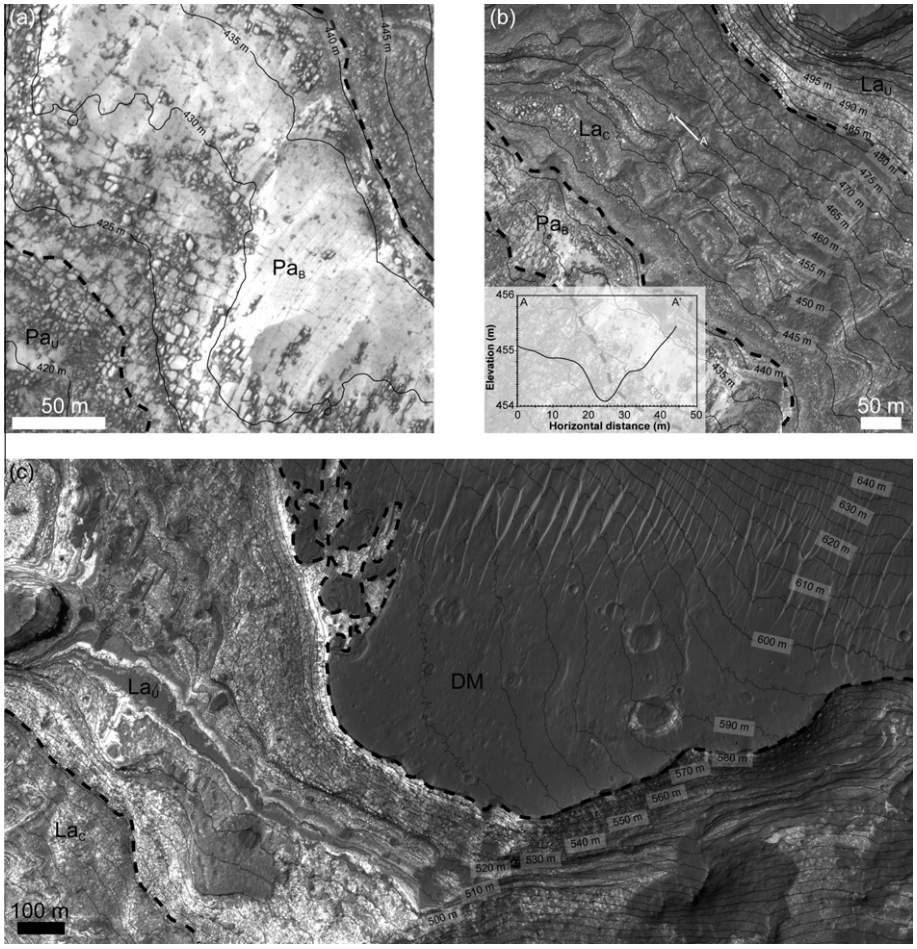

Fig. 11. HiRISE observations of LTDs in the upper part of the north wall of the trough. (a) LTDs units Pavement Upper (Pa_U) and Pavement Bright (Pa_B). (b) LTDs units Pavement Upper (Pa_U), Pavement Bright (Pa_B), Layered Channeled (La_C), and Layered Upper (La_U). Inset shows a topographic profile through a typical channel-like feature in La_C, indicated on the image by the solid white line. (c) LTDs units Layered Channeled (La_C), Layered Upper (La_U), and the dark mesa (DM) material. All images are taken from PSP_007917_1650 with north to the top of the images and 5 m contour intervals. In each image the dashed lines represent approximate boundaries between units.

be well constrained, where the age of the alteration is similar or younger to that of the LTDs. However, with the detrital hypothesis, the age and origin of the hydrous minerals are unknown. If they are derived from distal sources or from wall-rock material within the trough, their origin could be tied to some process of Noachian or Hesperian hydrous alteration that pre-dates the opening of Coprates Catena and deposition of the LTDs. This mechanism was shown to be the likely cause for the lacustrine phyllosilicate deposits in Jezero Crater, which were apparently sourced from smectite-rich regions in Nili Fossae (Ehlmann et al., 2008a), and also in the Uzboi–Ladon–Morava system (Milliken and Bish, 2010). However, the reported aqueous mineralogy of plateaus outside of Valles Marineris appears to be dominated by hydrated silica and sulfate, rather than hydroxylated silicate signatures (e.g. Milliken et al., 2008; Bishop et al., 2009; Weitz et al., 2008, 2010). We see no other external source for the input of sediments, aside from the small channels, and there are no observed hydration signatures in the wall of the trough. The possible presence of illite at the base of the observed sequence, which can form from the diagenetic alteration of Al-rich smectites (e.g. Ehlmann et al., 2009), also supports in situ alteration of the observed deposits. We therefore support the hypothesis that the hydrous minerals in Coprates Catena formed in situ, within the LTDs, a result of a Late Hesperian to Amazonian process.

Given the observations of flat-lying sediments that conform to the initial topography of the trough and the lack of evidence for externally-derived hydrous minerals, we describe possible scenarios and uncertainties regarding the formation and evolution of the LTDs. At some point following the formation of Coprates Catena, the trough became infilled with water. The origin of this water is unknown. However, the only two likely sources are groundwater and water derived from the trough-intersecting channels. There is no evidence of substantial gullying or fluvial dissection of the trough-interior slopes that might suggest a direct meteoric input. Unfortunately, no single observation can adequately demonstrate which source best explains infilling of the trough. The largest and possibly youngest channel that enters the trough deposited a large sedimentary fan (Di Achille et al., 2006; Weitz et al., 2006) that superposes the LTDs, and either formed as a sheetflood-dominated alluvial fan within a subaerial basin or by a deltaic depositional process within a lake. However, the shallow dips of the beds exposed within the fan indicate that if the fan was deposited as a delta, that the lake was likely of shallow water depth. The water involved in formation of this channel, along with water from older, shallow fluvial features that are truncated at the margins of the trough, may have contributed to episodic infilling of Coprates Catena, deposition of layered sediments, and hydrous alteration. The process of LTD deposition is equally unconstrained as we are unable to distinguish whether the LTDs were deposited by external sources in the absence of water (volcanic, aeolian, or fluvial) and subsequently altered by a later stage influx of water, or if a standing body of water (a lake) facilitated suspension, sedimentation

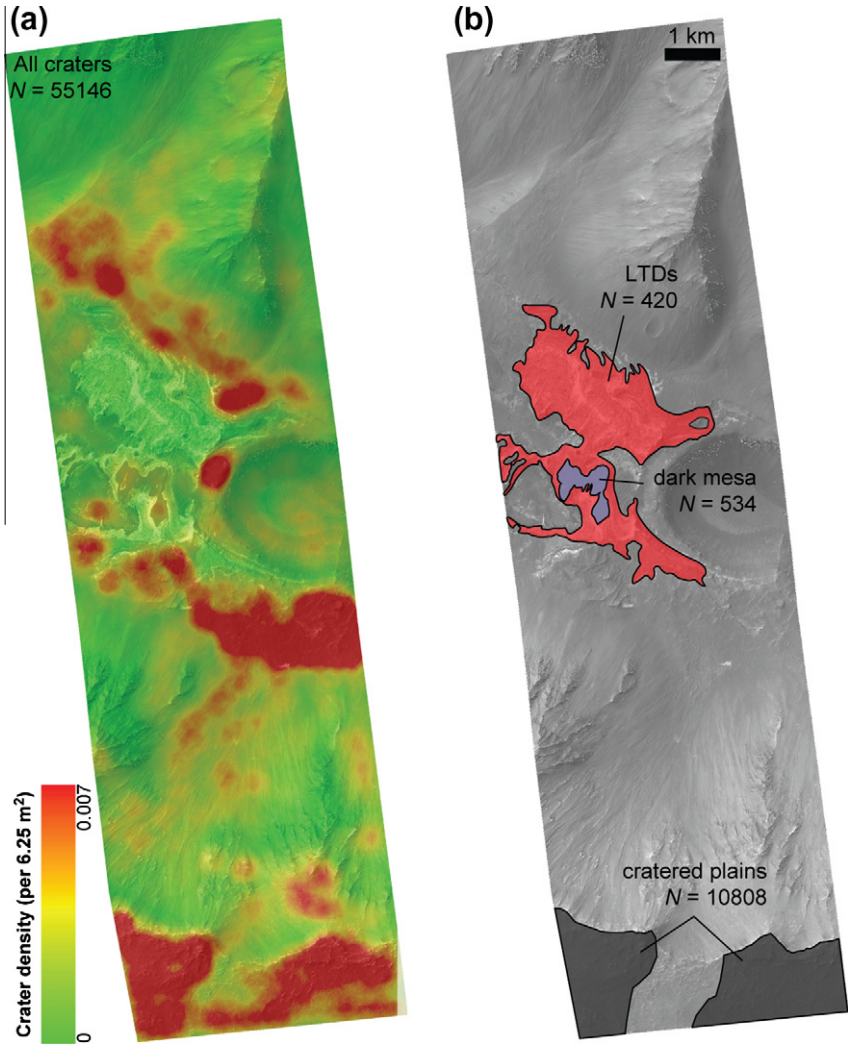

Fig. 12. Results of the HiRISE crater counting study. (a) Orthorectified HiRISE image PSP_007917_1650 overlain by a crater density map. The crater density was determined by counting all craters, regardless of size, in 6.25 m^2 grids, and highlights areas of low and high crater concentration. (b) The units used in the HiRISE crater counting study, with the number of craters identified in each unit, and plotted in Fig. 13.

and alteration. These issues are fundamental and common to all LTDs and interior layered deposits (ILDs) across Mars and will require in situ observations to differentiate between processes that fill basins with water, deposit sediments, and generate hydrous mineral phases.

Following, and possibly during, phases of water influx into the trough, a combination of evaporation and infiltration caused the water level to drop. As an ice-covered lake scenario cannot be ruled out, sublimation and ablation of the upper surface may have also led to volume loss. Our observations support the possibility that at least one phase of evaporation in the basin led to formation of a sulfate-bearing deposit (unit La_U) within the upper stratigraphic units. The fractures that are present throughout the LTDs could be evidence of evaporation processes (e.g. Weitz et al., 2008; El Maarry et al., 2010), although it is also possible that structural processes were responsible for fracturing. Following deposition of the sulfate-bearing material, dark-toned deposits were brought into the trough by erosion of the trough walls by small channels, with debris flows and channelization possibly responsible for forming the distinctive fan-like deposit covering the western end of the LTDs. However, as these deposits show no evidence of aqueous alteration, questions arise as to (1) whether these late stage fluvial events had any influence on aqueous alteration within the trough, (2) if previous floods into the trough were more voluminous and therefore involved more pervasive alteration, or (3) if alteration processes were exclusively limited to the basal units of the LTD stack? The last scenario would have been likely if groundwater, flowing into the basin at a defined topographic level, led to formation of hydrated basal sequences.

Several possible unconformities have been identified between units, particularly in the lower elevation units in the center of the trough. This observation suggests that throughout the time of trough infilling, surface water may have completely drained and/or evaporated, and once the LTDs were exposed, combined subaerial erosion and deposition of dark mantling material led to the formation of unconformities within the layered units. We see no definitive evidence of concentric fill impact craters within the stratigraphic sequence that could be suggestive of time breaks between deposition of individual units and long-standing formation of the LTDs (e.g. Michalski and Noe Dobrea, 2007), but most circular features on the modern surface of the LTDs, presumed to be impact craters, are heavily eroded and/or filled with dark mantling material. This suggests that the LTDs are relatively friable and easily eroded compared to the surface deposits of the surrounding highlands. The relatively high density of impact craters in the dark mantling material (Fig. 12) suggests that this unit underwent some

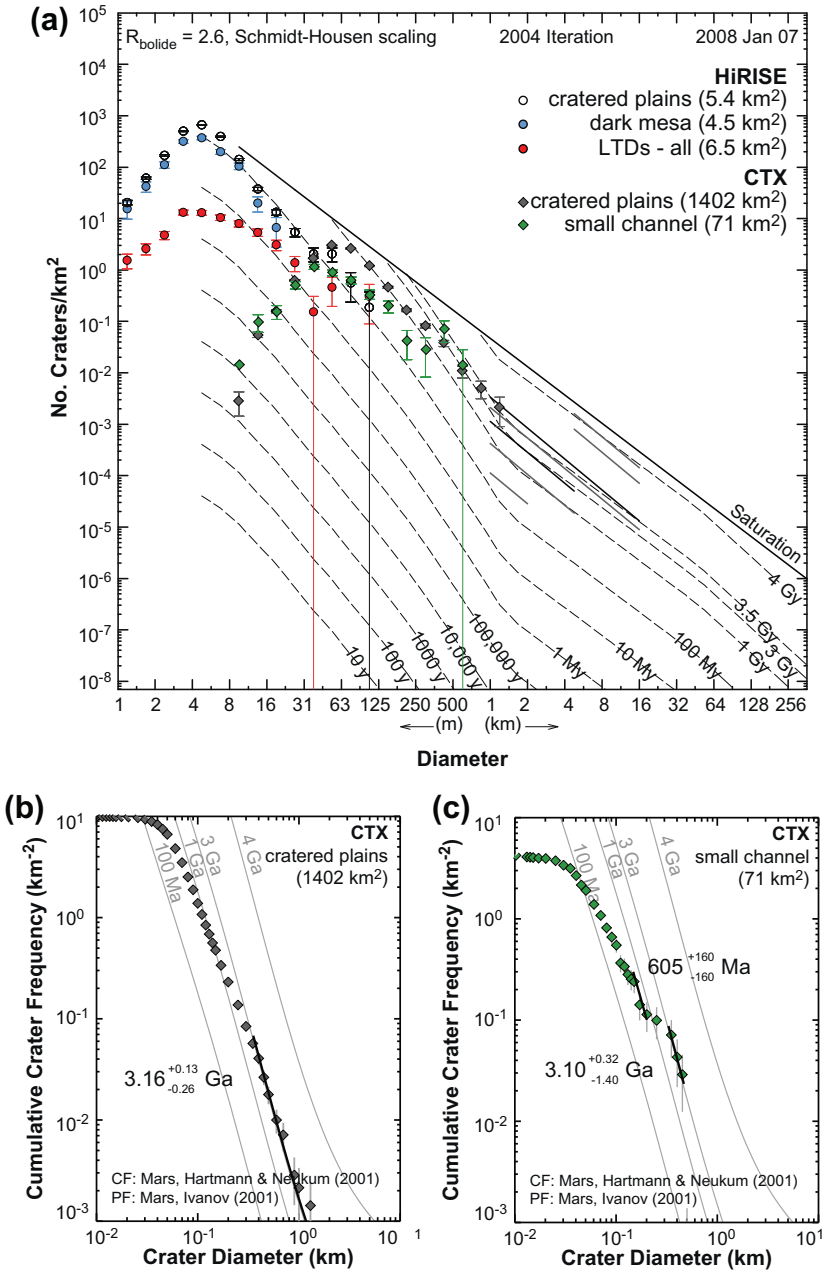

Fig. 13. Crater count plots from HiRISE and CTX crater counting surveys. (a) Crater count results for each of the HiRISE units shown in Fig. 12b, and also for larger representative units made using CTX images. The area of each unit is given in parentheses. The down-turn in smaller crater sizes is evident in the HiRISE and CTX units below about 5 and 30–40 m respectively. Scaling law relates the bolide diameter to crater diameter (Schmidt and Housen, 1987). (b) Binned cumulative crater frequency histogram for the cratered plains unit outside of the trough, made using CTX images. (c) Binned cumulative crater frequency histogram for the small channel unit that cuts the cratered plains unit outside of the trough, made using CTX images.

kind of induration, before ongoing erosion exhumed the LTDs to their present form.

Although our study does not help determine the source of any water that entered the trough, it does place limits on the possible maximum level of any standing water in the trough. We see no evidence, such as shorelines or terraces, on the walls of the trough above the LTDs to suggest that the maximum water depth was greater than the ~220 m implied by the thickness of the LTDs, although subsequent burial by mantling material could hide such evidence if not exhumed at a later date as with the LTDs. However, establishing water depths from sediment thicknesses is limited as progressive sedimentation in a basin with rising base level may have enabled accumulation of thick sedimentary successions even under relatively shallow water conditions. We will address the formation of the fan deposit in the west of the trough in detail in a future study, but we note some of the more important implications here. If water level in the trough was ever as high as the top of the fan deposit (Weitz et al., 2006), then it must have been ~1100 m higher than the top of our study LTDs, for which we see no evidence in the east of the trough. However, a similar low-lying small outcrop of LTDs is visible at the base of the north-west tip of the fan deposit, which occurs at the same elevation range as our study LTDs, between about 340 and 550 m. Further studies using HiRISE stereo and CRISM images, neither of which are currently available, are required to determine the detailed evolution of these accompanying LTDs, and whether they

are genetically linked to our study LTDs in the east of the trough. Of particular interest would be to determine whether the low elevation range of the LTDs is indicative of their formation in a shallow lake, a low energy deep water region (e.g. Milliken and Bish, 2010) prior to the fan deposit, or whether they represent alteration products of the original fan deposit (Fueten et al., 2010).

4.3. Implications for aqueous processes on Mars

Our identification of phyllosilicates as the dominant mineral species in the LTDs has major implications for our understanding of the chronology of aqueous alteration and the hydrologic history of Mars. Previous studies of LTDs in the Valles Marineris similar to those in this study have identified hydrated sulfates, both mono- and polyhydrated, as the major aqueous phase (e.g. Bishop et al., 2009; Flahaut et al., 2010; Fueten et al., 2010, 2011; Gendrin et al., 2005; Lichtenberg et al., 2010; Mangold et al., 2008; Murchie et al., 2009a,b; Roach et al., 2009). The locations of these sulfate hydrate deposits match well with predicted groundwater upwelling locations (e.g. Andrews-Hanna et al., 2007, 2010). However, some plateaus immediately surrounding parts of Valles Marineris do contain phyllosilicate phases and bear some resemblance to our LTDs. Similar light-toned deposits, often layered, containing phyllosilicates, sulfates and opaline silica have recently been identified adjacent to Ius, Melas, Candor, Juventae, and Ganges Chasmae (Bishop et al., 2009; Le Deit et al., 2010; Roach et al., 2010; Weitz et al., 2010), and Noctis Labyrinthus (Weitz et al., 2011), but to date, similar deposits have not been recorded around the Coprates region. The identification of such sequences of combined composition are even rarer within the canyons and troughs of Valles Marineris, with the apparent transition from a neutral to acidic environment inferred at Ius Chasma by Roach et al. (2010) and Noctis Labyrinthus (Weitz et al., 2011) offering to date the only other similar sequences to that identified here.

Despite the identification of phyllosilicates with some sulfates within Valles Marineris-type layered deposits being rare, the possible mineralogy that we have observed is not without precedent on Mars. The combination of phyllosilicates and sulfates located in a draped succession on the walls of our study trough are most compatible with the intracrater clay–sulfate deposits described by Murchie et al. (2009a), which generally contain the Al phyllosilicate kaolinite and hydrated sulfates. This class of deposits is most common in craters in Terra Sirenum, rather than Valles Marineris, with the type example in Columbus Crater (Murchie et al., 2009a; Wray et al., 2011). The identification of Al phyllosilicates interbedded with sulfate hydrate phases, and accompanying structural analysis, led Wray et al. (2011) to favor a deep lake setting for formation of the light-toned deposits in Columbus Crater. The overall mineral sequence of Columbus Crater also agreed reasonably well with geochemical models of evaporation of deep lakes on Mars (e.g. Altheide et al., 2010), with sulfate minerals forming predominantly from a playa-lake type environment and phyllosilicates forming mainly from groundwater action (Wray et al., 2011).

Although there are some notable similarities between the LTDs in Columbus Crater and our study trough, there are at least three important differences. The first difference is that the putative lake that might have led to the formation of the LTDs was probably only up to ~220 m deep, at least at the eastern end of the trough, rather than 900 m postulated for Columbus Crater (Wray et al., 2011). The second difference is that we do not see interbedded phyllosilicates and sulfates throughout the layered sequence, rather the LTDs contain predominantly Al phyllosilicates, with a discrete band of Fe/Mg phyllosilicates, and possibly the appearance of hydrated sulfate or silica minerals towards the top of the deposits. Our identification of Al phyllosilicates underlying Fe/Mg phyllosilicates is also rare on Mars, with the opposite sequence being more common and attributed to surface weathering (e.g. Wray et al., 2009), although a similar stratigraphic sequence has also recently been identified in Noctis Labyrinthus (Weitz et al., 2011). Finally, the apparent age of the LTDs appears to be Late Hesperian to Early Amazonian, rather than Late Noachian as in Columbus Crater (Wray et al., 2011). Given the lack of evidence for clay minerals within possible bedrock source regions, we posit that the clays in Coprates Catena were formed in situ and therefore are also Late Hesperian to Early Amazonian in age.

The current paradigm regarding the evolution of the water chemistry on Mars, and the subsequent dominant alteration products, involves relatively large volumes of near-neutral pH water in the Noachian, leading to the formation of phyllosilicate assemblages, before reduced volumes of more acidic water led to the formation of predominantly sulfate minerals during the Hesperian (Bibring et al., 2006). If our observations are correct, then they do not fit easily into the current paradigm regarding water on Mars. However, as noted by Murchie et al. (2009a), although many observations support the paradigm of Bibring et al. (2006), there are so far two notable exceptions, namely: (1) the kaolinite–sulfate assemblages that suggest that phyllosilicate and sulfate formation overlapped in time and space, at least in some highland craters, and (2) the recent discoveries of ancient carbonate deposits (e.g. Ehlmann et al., 2008b, 2009) suggests that the transition to acidic conditions might not have been globally pervasive. Further work at other similar LTDs is necessary to determine whether the potentially relatively young phyllosilicates identified here and possibly elsewhere in Valles Marineris (e.g. Roach et al., 2010; Weitz et al., 2011) are localized deposits, or represent a more extensive set of deposits that could be additional exceptions to the hypothesis of Bibring et al. (2006).

5. Conclusions

We have analyzed the mineralogy and stratigraphy of an approximately 220 m thick succession of light-toned deposits (LTDs) in a small trough in Coprates Catena. Using CRISM data we have identified material containing phyllosilicates, and sulfates and/or opaline silica associated with the LTDs that appear to represent a sequence of dominant mineralogies. With increasing height from the observable base of the LTDs, we see Al phyllosilicates, a band of Fe/Mg phyllosilicates, Al phyllosilicates, and finally sulfate hydrates and/or opaline silica at the top of the LTDs. Using a HiRISE DEM we have determined that individual layers on both sides of the trough dip gently towards the center of the trough with a dip direction that matches that of the trough. The combined mineralogy and morphology of the LTDs match well with formation as a sedimentary basin in a closed depositional system. The general order of events in our study trough are: (1) opening of trough, (2) water enters the trough (3) water loss leads to possibly repeated episodes of phyllosilicate deposition/formation and increasing evaporite precipitation, (4) dark mantling material buries LTDs and becomes indurated, (5) formation of collapse pits in base of trough, (6) ongoing exhumation and erosion of dark mantling material and LTDs. Crater statistics do not allow us to date the LTDs themselves, but we can determine a likely upper age based on the timing of trough formation at around 3.16 Ga. If this age is accurate then these LTDs could represent a new class of deposit made up of Late Hesperian/Early Amazonian phyllosilicate deposits, although we cannot rule out an allochthonous origin for the observed mineralogy. However, our results do suggest that this trough, and perhaps other closed troughs in Valles Marineris that contain similar LTDs, likely contained significant amounts of water towards the end of the Hesperian, postdating most of the major tectonic activity.

Acknowledgments

We thank Matt Balme and Elliot Sefton-Nash for discussions about crater statistics and CRISM summary profiles, and Chris Okubo for advice on structural analysis techniques, as well as Laetitia Le Deit and an anonymous reviewer for thorough reviews and constructive comments. We also thank the CTX, HiRISE and CRISM teams for making the data available, and providing tools to aid in their processing. The HiRISE DEM and CRISM processing was carried out at the UK NASA RPIF at University College London. P.M.G. is funded by an STFC Aurora Fellowship (Grant ST/F011830/1), and thanks the Royal Astronomical Society and the UCL Graduate School for travel funds. N.H.W. and S.G. were funded by STFC Grant ST/F003099/1.

References

Adams, J.B. et al., 2009. Salt tectonics and collapse of Hebes Chasma, Valles Marineris, Mars. Geology 37, 691–694. doi:10.1130/G30024A.1.

Altheide, T.S., Chevrier, V.F., Rivera-Valentin, E.G., Wray, J.J., 2010. Geochemical modeling of the evaporation of an ancient paleolake in Columbus crater, Terra Sirenum, Mars. Lunar Planet. Sci. XLII. Abstract 2479.

Andrews-Hanna, J.C., Phillips, R.J., Zuber, M.T., 2007. Meridiani Planum and the global hydrology of Mars. Nature 446, 163–166. doi:10.1038/nature05594.

Andrews-Hanna, J.C., Zuber, M.T., Arvidson, R.E., Wiseman, S.M., 2010. Early Mars hydrology: Meridiani playa deposits and the sedimentary record of Arabia Terra. J. Geophys. Res. 115, E06002. doi:10.1029/2009JE003485.

Baioni, D., Wezel, F.C., 2010. Morphology and origin of an evaporitic dome in the eastern Tithonium Chasma, Mars. Planet. Space Sci. 58, 847–857. doi:10.1016/j.pss.2010.01.009.

Bibring, J.-P. et al., 2006. Global mineralogical and aqueous Mars history derived from OMEGA/Mars Express data. Science 312, 400–404. doi:10.1126/science.1122659.

Bishop, J.L., Lane, M.D., Dyar, M.D., Brown, A.J., 2008. Reflectance and emission spectroscopy study of four groups of phyllosilicates: Smectites, kaolinite–serpentines, chlorites and micas. Clay Miner. 43, 35–54. doi:10.1180/claymin.2008.043.1.03.

Bishop, J.L. et al., 2009. Mineralogy of Juventae Chasma: Sulfates in the light-toned mounds, mafic minerals in the bedrock, and hydrated silica and hydroxylated ferric sulfate on the plateau. J. Geophys. Res. 114, E00D09. doi:10.1029/2009JE003352.

Bristow, T.F., Milliken, R.E., 2011. The use of mineral facies models of terrestrial saline lakes as potential guides to the origin of martian phyllosilicates. Lunar Planet. Sci. XLII. Abstract 2457.

Catling, D.C., Wood, S.E., Leovy, C., Montgomery, D.R., Greenberg, H.M., Glein, C.R., Moore, J.M., 2006. Light-toned deposits in Juventae Chasma, Mars. Icarus 181, 26–51. doi:10.1016/j.icarus.2005.10.020.

Chapman, M.G., Tanaka, K.L., 2001. Interior trough deposits on Mars: Subice volcanoes? J. Geophys. Res. 106, 10087–10100. doi:10.1029/2000JE001303.

Clark, R.N. et al., 2007. USGS digital spectral library splib06a. US Geol. Sur., Dig. Data Ser., 231. <http://speclab.cr.usgs.gov/spectral.lib06>.

Di Achille, G. et al., 2006. A steep fan at Coprates Catena, Valles Marineris, Mars, as seen by HRSC data. Geophys. Res. Lett. 33, L07204. doi:10.1029/2005GL025435.

Ehlmann, B.L. et al., 2008a. Clay minerals in delta deposits and organic preservation potential on Mars. Nat. Geosci. 1, 355–358. doi:10.1038/ngeo207.

Ehlmann, B.L. et al., 2008b. Orbital identification of carbonate-bearing rocks on Mars. Science 322, 1828–1832. doi:10.1126/science.1164759.

Ehlmann, B.L. et al., 2009. Identification of hydrated silicate minerals on Mars using MRO-CRISM: Geologic context near Nili Fossae and implications for aqueous alteration. J. Geophys. Res. 114, E00D08. doi:10.1029/2009JE003339.

El Maarry, M.R., Markiewicz, W.J., Mellon, M.T., Goetz, W., Dohm, J.M., Pack, A., 2010. Crater floor polygons: Desiccation patterns of ancient lakes on Mars? J. Geophys. Res. 115, E10006. doi:10.1029/2010JE003609.

Flahaut, J., Quantin, C., Allemand, P., Thomas, P., Le Deit, L., 2010. Identification, distribution and possible origins of sulfates in Capri Chasma (Mars), inferred from CRISM data. J. Geophys. Res. 115, E11007. doi:10.1029/2009JE003566.

Fueten, F., Stesky, R.M., MacKinnon, P., 2005. Structural attitudes of large scale layering in Valles Marineris, Mars, calculated from Mars Orbiter Laser Altimeter data and Mars Orbiter Camera imagery. Icarus 175, 68–77. doi:10.1016/j.icarus.2004.11.010.

Fueten, F. et al., 2008. Stratigraphy and structure of interior layered deposits in west Candor Chasma, Mars, from High Resolution Stereo Camera (HRSC) stereo imagery and derived elevations. J. Geophys. Res. 113, E10008. doi:10.1029/2007JE003053.

Fueten, F. et al., 2010. Structural analysis of interior layered deposits in Northern Coprates Chasma, Mars. Earth Planet. Sci. Lett. 294, 343–356. doi:10.1016/j.epsl.2009.11.004.

Fueten, F., Flahaut, J., Le Deit, L., Stesky, R., Hauber, E., Gwinner, K., 2011. Interior layered deposits within a perched basin, southern Coprates Chasma, Mars: Evidence for their formation, alteration, and erosion. J. Geophys. Res. 116, E02003. doi:10.1029/2010JE003695.

Gendrin, A. et al., 2005. Sulfates in martian layered terrains: The OMEGA/Mars Express view. Science 307, 1587–1591. doi:10.1126/science.1109087.

Grindrod, P.M., Balme, M.R., 2010. Groundwater processes in Hebes Chasma, Mars. Geophys. Res. Lett. 37, L13202. doi:10.1029/2010GL044122.

Grindrod, P.M. et al., 2010. Experimental investigation of the mechanical properties of synthetic magnesium sulfate hydrates: Implications for the strength of hydrated deposits on Mars. J. Geophys. Res. 115, E06012. doi:10.1029/2009JE003552.

Harrison, K.P., Chapman, M.G., 2008. Evidence for ponding and catastrophic floods in central Valles Marineris, Mars. Icarus 198, 351–364. doi:10.1016/j.icarus.2008.08.003.

Hartmann, W.K., 2005. Martian cratering 8: Isochron refinement and the chronology of Mars. Icarus 174, 294–320. doi:10.1016/j.icarus.2004.11.023.

Hartmann, W.K., Neukum, G., 2001. Cratering chronology and the evolution of Mars. Space Sci. Rev. 96, 165–194. doi:10.1023/A:1011945222010.

Hunt, G.R., Ashley, R.P., 1979. Spectra of altered rocks in the visible and near-infrared. Econ. Geol. 74, 1613–1629. doi:10.2113/gsecongeo.74.7.1613.

Ivanov, B.A., 2001. Mars/Moon cratering rate ratio estimates. Space Sci. Rev. 96, 87–104. doi:10.1023/A:1011941121102.

Jackson, M.P.A., Adams, J.B., Dooley, T.P., Gillespie, A.R., Montgomery, D.R., 2011. Modeling the coll of Hebes Chasma, Valles Marineris, Mars. Geol. Soc. Am. Bull., in press. doi:10.1130/B30307.1.

King, T.V.V., Clark, R.N., 1989. Spectral characteristics of chlorites and Mg-serpentines using high-resolution reflectance spectroscopy. J. Geophys. Res. 94, 13997–14008. doi:10.1029/JB094iB10p13997.

Kirk, R.L. et al., 2008. Ultra-high-resolution topographic mapping of Mars with MRO HiRISE stereo images: Meter-scale slopes of candidate Phoenix landing sites. J. Geophys. Res. 113, E00A24. doi:10.1029/2007JE003000.

Komatsu, G., Geissler, P.E., Strom, R.G., Singer, R.B., 1993. Stratigraphy and erosional landforms of layered deposits in Valles Marineris. J. Geophys. Res. 98, 11105–11121. doi:10.1029/93JE00537.

Komatsu, G., Ori, G.G., Ciarcelluti, P., Litasov, Y.D., 2004. Interior layered deposit of Valles Marineris, Mars: Analogous subice volcanism related to Baikal Rifting, Southern Siberia. Planet. Space Sci. 52, 167–187. doi:10.1016/j.pss.2003.08.003.

Le Deit, L., Bourgeois, O., Mège, D., Hauber, E., Mouélic, Le, Massé, M., Jaumann, R., Bibring, J.-P., 2010. Morphology, stratigraphy, and mineralogical composition of a layered formation covering the plateaus around Valles Marineris, Mars: Implications for its geological history. Icarus 208, 684–703. doi:10.1016/j.icarus.2010.03.012.

Lichtenberg, K.A. et al., 2010. Stratigraphy of hydrated sulfates in the sedimentary deposits of Aram Chaos, Mars. J. Geophys. Res. 115, E00D17. doi:10.1029/2009JE003353.

Lucchitta, B.K., 2009a. Lakes in Valles Marineris, Mars (I): Walls, mounds, moats, and volcanoes. Lunar Planet. Sci. XL. Abstract 2068.

Lucchitta, B.K., 2009b. Lakes in Valles Marineris, Mars (II): Valleys, channels, shallow lakes, and age. Lunar Planet. Sci. XL. Abstract 2345.

Lucchitta, B.K. et al., 1992. The canyon system on Mars. In: Kieffer, H.H., Jakosky, B.M., Snyder, C.W., Matthews, M.S. (Eds.), Mars. Univ. Ariz. Press, Tucson, pp. 453–492.

Lucchitta, B.K., Isbell, N.K., Howington-Kraus, A., 1994. Topography of Valles Marineris: Implications for erosional and structural history. J. Geophys. Res. 99, 3783–3798. doi:10.1029/93JE03095.

Malin, M.C., Edgett, K.S., 2000. Sedimentary rocks of early Mars. Science 290, 1927–1937. doi:10.1126/science.290.5498.1927.

Malin, M.C., Edgett, K.S., 2001. Mars Global Surveyor Mars Orbiter Camera: Interplanetary cruise through primary mission. J. Geophys. Res. 106, 23429–23570. doi:10.1029/2000JE001455.

Malin, M.C., Edgett, K.S., 2003. Evidence for persistent flow and aqueous sedimentation on early Mars. Science 302, 1931–1934. doi:10.1126/science.1090544.

Malin, M.C. et al., 2007. Context camera investigation on board the Mars Reconnaissance Orbiter. J. Geophys. Res. 112, E05S04. doi:10.1029/2006JE002808.

Mangold, N., Gendrin, A., Gondet, B., LeMouelic, S., Quantin, C., Ansan, V., Bibring, J.-P., Langevin, Y., Masson, P., Neukum, G., 2008. Spectral and geological study of the sulfate-rich region of West Candor Chasma, Mars. Icarus 194, 519–543. doi:10.1016/j.icarus.2007.10.021.

McCauley, J.F., 1978. Geologic map of the Coprates Quadrangle of Mars, scale 1:5,000,000. US Geol. Surv. Misc. Inv. Ser., Map I-897.

McCauley, J.F., Carr, M.H., Cutts, J.A., Hartmann, W.K., Masursky, H., Milton, D.J., Sharp, R.P., Wilhelms, D.E., 1972. Preliminary Mariner 9 report on the geology of Mars. Icarus 17, 289–327. doi:10.1016/0019-1035(72)90003-6.

McEwen, A.S., 2003. Secondary cratering on Mars: Implications for age dating and surface properties. Mars Polar Ice Conf. III. Abstract 3268.

McEwen, A.S., Preblich, B.S., Turtle, E.P., Artemieva, N.A., Golombek, M.P., Hurst, M., Kirk, R.L., Burr, D.M., Christensen, P.R., 2005. The rayed crater Zunil and interpretations of small impact craters on Mars. Icarus 176, 351–381. doi:10.1016/j.icarus.2005.02.009.

McGuire, P.C. et al., 2009. An improvement to the volcano-scan algorithm for atmospheric correction of CRISM and OMEGA spectral data. Planet. Space Sci. 57, 809–815. doi:10.1016/j.pss.2009.03.007.

Mège, D., Cook, A.C., Garel, E., Lagabrielle, Y., Cormier, M.-H., 2003. Volcanic rifting at martian grabens. J. Geophys. Res. 108, 5044. doi:10.1029/2002JE001852.

Michalski, J.R., Noe Dobrea, E.Z., 2007. Evidence for a sedimentary origin of clay minerals in the Mawrth Vallis region, Mars. Geology 35, 951–954. doi:10.1130/G23854A.1.

Milliken, R.E., Bish, D.L., 2010. Sources and sinks of clay minerals on Mars. Philos. Mag. 90, 14–28. doi:10.1080/1478643090375132.
Milliken, R.E. et al., 2008. Opaline silica in young deposits on Mars. Geology 36, 847–850. doi:10.1130/G24967A.1.
Milliken, R.E., Grotzinger, J.P., Thomson, B.J., 2010. Paleoclimate of Mars as captured by the stratigraphic record in Gale Crater. Geophys. Res. Lett. 37, L04201. doi:10.1029/2009GL041870.
Montgomery, D.R., Gillespie, A., 2005. Formation of martian outflow channels by catastrophic dewatering of evaporite deposits. Geology 33, 625–628. doi:10.1130/G21270.1.
Montgomery, D.R., Som, S.M., Jackson, M.P.A., Schreiber, B.C., Gillespie, A.R., Adams, J.B., 2009. Continental-scale salt tectonics on Mars and the origin of Valles Marineris and associated outflow channels. Geol. Soc. Am. Bull. 121, 117–133. doi:10.1130/B26307.1.
Murchie, S. et al., 2007. Compact Reconnaissance Imaging Spectrometer for Mars (CRISM) on Mars Reconnaissance Orbiter (MRO). J. Geophys. Res. 112, E05S03. doi:10.1029/2006JE002682.
Murchie, S. et al., 2009a. A synthesis of martian aqueous mineralogy after 1 Mars year of observations from the Mars Reconnaissance Orbiter. J. Geophys. Res. 114, E00D06. doi:10.1029/2009JE003342.
Murchie, S. et al., 2009b. Evidence for the origin of layered deposits in Candor Chasma, Mars, from mineral composition and hydrologic modeling. J. Geophys. Res. 114, E00D05. doi:10.1029/2009JE003343.
Mustard, J.F. et al., 2008. Hydrated silicate minerals on Mars observed by the Mars Reconnaissance Orbiter CRISM instrument. Nature 454, 305–309. doi:10.1038/nature07097.
Nedell, S.S., Squyres, S.W., Andersen, D.W., 1987. Origin and evolution of the layered deposits in the Valles Marineris, Mars. Icarus 70, 409–414. doi:10.1016/0019-1035(87)90086-8.
Okubo, C.H., 2010. Structural geology of Amazonian-aged layered sedimentary deposits in southwest Candor Chasma, Mars. Icarus 207, 210–225. doi:10.1016/j.icarus.2009.11.012.
Okubo, C.H., Lewis, K.W., McEwen, A.S., Kirk, R.L., 2008. Relative age of interior layered deposits in southwest Candor Chasma based on high-resolution structural mapping. J. Geophys. Res. 113, E12002. doi:10.1029/2008JE003181.
Pelkey, S.M. et al., 2007. CRISM multispectral summary products: Parameterizing mineral diversity in Mars from reflectance. J. Geophys. Res. 112, E08S14. doi:10.1029/2006JE002831.
Peterson, C., 1981. A secondary origin for the central plateau of Hebes Chasma. Proc. Lunar Sci. Conf. 11, 1459–1471.
Roach, L.H. et al., 2009. Testing evidence of recent hydration state change in sulfates on Mars. J. Geophys. Res. 114, E00D02. doi:10.1029/2008JE003245.
Roach, L.H., Mustard, J.F., Swayze, G., Milliken, R.E., Bishop, J.L., Murchie, S.L., Lichtenberg, K., 2010. Hydrated mineral stratigraphy of Ius Chasma, Valle Marineris. Icarus 206, 253–268. doi:10.1016/j.icarus.2009.09.003.
Schmidt, R.M., Housen, K.R., 1987. Some recent advances in the scaling of impact and explosion cratering. Int. J. Impact Eng. 5, 543–560. doi:10.1016/0734-743X(87)90069-8.
Schultz, R.A., 1991. Structural development of Coprates Chasma and Western Ophir Planum, Valles Marineris Rift, Mars. J. Geophys. Res. 96, 22777–22792. doi:10.1029/91JE02556.
Schultz, R.A., 1998. Multiple-process origin of Valles Marineris basins and troughs, Mars. Planet. Space Sci. 46, 827–834. doi:10.1016/S0032-0633(98)00030-0.
Scott, D.H., Tanaka, K.L., 1986. Geologic map of the western equatorial region of Mars. US Geol. Surv. Misc. Invest. Ser., Map, I-1802-A.
Sharp, R.P., 1973. Mars: Troughed terrain. J. Geophys. Res. 78, 4063–4072. doi:10.1029/JB078i020p04063.
Smith, D.E. et al., 2001. Mars Orbiter Laser Altimeter (MOLA): Experiment summary after the first year of global mapping of Mars. J. Geophys. Res. 106, 23689–23722. doi:10.1029/2000JE001364.
Warner, N.H., Farmer, J.D., 2010. Subglacial hydrothermal alteration minerals in jökulhlaup deposits of Southern Iceland, with implications for detecting past or present habitable environments on Mars. Astrobiology 10, 523–547. doi:10.1089/ast.2009.0425.
Weitz, C.M., Irwin, R.P., Chuang, F.C., Bourke, M.C., Crown, D.A., 2006. Formation of a terraced fan deposit in Coprates Catena, Mars. Icarus 184, 436–451. doi:10.1016/j.icarus.2006.05.024.
Weitz, C.M., Milliken, R.E., Grant, J.A., McEwen, A.S., Williams, R.M.E., Bishop, J.L., 2008. Light toned strata and inverted channels adjacent to Juventae and Granges chasmata, Mars. Geophys. Res. Lett. 35, L19202. doi:10.1029/2008GL035317.
Weitz, C.M., Milliken, R.E., Grant, J.A., McEwen, A.S., Williams, R.M.E., Bishop, J.L., Thomson, B.J., 2010. Mars Reconnaissance Orbiter observations of light-toned layered deposits and associated fluvial landforms on the plateaus adjacent to Valles Marineris. Icarus 205, 73–102. doi:10.1016/j.icarus.2009.04.017.
Weitz, C.M., Bishop, J.L., Thollot, P., Mangold, N., Roach, L.H., 2011. Diverse mineralogies in two troughs of Noctis Labyrinthus, Mars. Geology, in press. doi:10.1130/G32045.1.
Wiseman, S.M. et al., 2010. Spectral and stratigraphic mapping of hydrated sulfate and phyllosilicate-bearing deposits in northern Sinus Meridiani, Mars. J. Geophys. Res. 115, E00D18. doi:10.1029/2009JE003354.
Wray, J.J., Murchie, S.M., Squyres, S.W., Seelos, F.P., Tornabene, L.L., 2009. Diverse aqueous environments on ancient Mars revealed in the southern highlands. Geology 37, 1043–1046. doi:10.1130/G30331A.1.
Wray, J.J. et al., 2011. Columbus crater and other possible groundwater-fed paleolakes of Terra Sirenum, Mars. J. Geophys. Res. 116, E01001. doi:10.1029/2010JE003694.